catalysts

MDPI

Article

Hydrogen Production by Ethanol Steam Reforming (ESR) over CeO_2 Supported Transition Metal (Fe, Co, Ni, Cu) Catalysts: Insight into the Structure-Activity Relationship

Michalis Konsolakis [1], Zisis Ioakimidis [2,3], Tzouliana Kraia [2,3] and George E. Marnellos [2,3,4,*]

1 School of Production Engineering and Management, Technical University of Crete, GR-73100 Chania, Crete, Greece; mkonsol@science.tuc.gr (M.K.)
2 Department of Mechanical Engineering, University of Western Macedonia, Bakola & Sialvera, GR-50100 Kozani, Greece; zisis.ioakimidis@hotmail.com (Z.I.); jouliana.kraia.uowm@gmail.com (Tz.K.)
3 Chemical Process & Energy Resources Institute, Centre for Research & Technology Hellas, 6th km. Charilaou—Thermi Rd., P.O. Box 60361, GR-57001 Thermi, Thessaloniki, Greece
4 Department of Environmental Engineering, University of Western Macedonia, Bakola & Sialvera, GR-50100 Kozani, Greece
* Correspondence: gmarnellos@uowm.gr; Tel.: +30-24610-56690; Fax: +30-24610-56601

Academic Editor: Keith Hohn
Received: 30 November 2015; Accepted: 2 March 2016; Published: 8 March 2016

Abstract: The aim of the present work was to investigate steam reforming of ethanol with regard to H_2 production over transition metal catalysts supported on CeO_2. Various parameters concerning the effect of temperature (400–800 °C), steam-to-carbon (S/C) feed ratio (0.5, 1.5, 3, 6), metal entity (Fe, Co, Ni, Cu) and metal loading (15–30 wt.%) on the catalytic performance, were thoroughly studied. The optimal performance was obtained for the 20 wt.% Co/CeO_2 catalyst, achieving a H_2 yield of up to 66% at 400 °C. In addition, the Co/CeO_2 catalyst demonstrated excellent stability performance in the whole examined temperature range of 400–800 °C. In contrast, a notable stability degradation, especially at low temperatures, was observed for Ni-, Cu-, and Fe-based catalysts, ascribed mainly to carbon deposition. An extensive characterization study, involving N_2 adsorption-desorption (BET), X-ray diffraction (XRD), Scanning Electron Microscopy (SEM/EDS), X-ray Photoelectron Spectroscopy (XPS), and Temperature Programmed Reduction (H_2-TPR) was undertaken to gain insight into the structure-activity correlation. The excellent reforming performance of Co/CeO_2 catalysts could be attributed to their intrinsic reactivity towards ethanol reforming in combination to their high surface oxygen concentration, which hinders the deposition of carbonaceous species.

Keywords: ethanol steam reforming; H_2 production; ceria-based catalysts; iron; cobalt; nickel; copper; XPS; H_2-TPR; stability

1. Introduction

Energy is a vital element in our everyday lives, mostly generated, however, from fossil fuels. Furthermore, our continuous dependence on fossil fuels is strongly coupled with natural resource depletion and serious environmental implications, such as greenhouse effect, stratospheric ozone depletion, photochemical smog, *etc*. Therefore, the need for renewable energy is becoming ever more urgent. In view of this fact, solar, wind, and biomass have become promising renewable energy sources (RES). Although significant technological progress has been accomplished in their efficient energy conversion, their share in the world energy mix is limited due to their intermittent character and site-dependence. On the other hand, hydrogen has been acknowledged as an ideal energy currency

for sustainable energy development. Hydrogen can be employed as feedstock in a fuel cell to directly generate electricity at high efficiencies and low environmental footprint. In this regard, hydrogen production in a clean and renewable manner is essential for a sustainable energy future [1–4].

Nowadays, the steam reforming of natural gas is the most frequently employed and economically feasible method for hydrogen production [1–3]. This process, however, is based on a fossil resource and is linked with CO_2 emissions, unless carbon capture and storage (CCS) techniques are employed, which inevitably increase the complexity and overall costs. The rising concerns, related to the reduction of atmospheric pollutants in conjunction with the continuously increasing energy demands, have stimulated the research toward hydrogen production from renewable sources. In this direction, ethanol is among the most promising feedstocks, due to its relatively high hydrogen content, wide availability, non-toxicity, as well as storage and handling safety. Moreover, ethanol can be generated in a renewable manner through biomass (energy crops, agricultural and industrial wastes, forestry residues, and the organic fraction of municipal solid waste) fermentation [5–7]. The employment of bio-fuels in hydrogen production incorporates important environmental advantages, since the generated CO_2 can be recycled through photosynthesis during plant growth, resulting in a carbon neutral process.

Hydrogen production by reforming processes is usually achieved either by steam or auto-thermal reforming. Compared to auto-thermal reforming, ethanol steam reforming (ESR) has received more focus due to the higher H_2 yields obtained through this route [8–12]:

$$CH_3CH_2OH_{(g)} + 3H_2O_{(g)} \rightarrow 6H_{2(g)} + 2CO_{2(g)},\ \Delta H^0{}_{298} = +173.1\ \text{kJ/mol} \quad (1)$$

Furthermore, the water gas shift (WGS) reaction, taking place at excess H_2O conditions, can further increase the H_2 yield:

$$CO_{(g)} + H_{2O_{(g)}} \rightarrow CO_{2(g)} + H_{2(g)},\ \Delta H^0{}_{298} = -41\ \text{kJ/mol} \quad (2)$$

Nevertheless, the overall reforming process consists of a complex network of reactions, such as ethanol dehydrogenation, dehydration, or decomposition, which can lead to the formation of several byproducts (methane, ethylene, acetaldehyde, acetone, coke, *etc.*) [10,13].

Furthermore, technological advances in the direct utilization of bio-fuels, like bio-ethanol, in Solid Oxide Fuel cells (SOFCs) have stimulated the research toward the development of high efficiency fuel processing electro-catalysts with adequate activity and durability. Under these perspectives, several catalytic systems, involving mainly base (e.g., Ni, Co, Cu) and precious (e.g., Pt, Rh, Ru, Pd, and Ir) metal supported catalysts have been reported for ESR [10,12]. Although the noble metal-based catalysts demonstrate sufficient reforming activity in a wide temperature range [10,12,14–19], their large-scale implementation in practice is limited by their significant high cost [20]. Hence, the development of active and stable non-precious metal catalysts for ESR is highly desirable. Ni-based catalysts are the most commonly employed catalytic systems, due to their inherent activity on C-C and C-H bond cleavage [21]. However, their insufficient tolerance to carbon deposition in conjunction with the sintering of Ni particles at elevated temperatures, have been considered the main barriers for industrial application [22]. Recent studies, however, have shown that highly active and stable Ni-based catalysts can be obtained by appropriately adjusting their physicochemical properties by means of advanced synthesis procedures and/or structural/surface promotion (e.g., [23,24]). Strong Ni-ceria interactions can be accounted for the enhanced ESR activity [25–27].

Regarding the catalyst support, it should generally possess adequate chemical and mechanical properties to provide the required activity and stability under reaction conditions. Most importantly, supporting carriers should provide strong metal-support interactions and high oxygen mobility (redox properties), preserving the active phase from sintering and coking deactivation. Ceria has been widely employed in several catalytic reactions, involving the WGS reaction [28], NOx reduction [29,30], oxidation or partial oxidation of hydrocarbons [31], steam reforming [32], *etc.*, owing to its excellent redox properties. The mobile oxygen related to the ceria lattice, is considered to be responsible

for the oxidation of deposited carbonaceous fragments, thus protecting the catalyst surface from poisoning [33–36]. In addition, mobile oxygen can activate water, with regard to the formation of hydroxyl groups, resulting in higher ESR efficiency [25,33]. In a comprehensive study by Xu *et al.* [25], utilizing both *in situ* and *ex situ* characterization techniques it was revealed that metallic Ni and Ce(III) entities were the active components under ESR conditions. Ce(III) facilitates the decomposition of H_2O to –OH groups, which are essential for the transformation of $C_xH_yO_z$ intermediates to CO_2 and H_2O, whereas Ni promotes the adsorption of ethanol and dissociation of C–C bonds. Moreover, strong Ni-ceria interactions perturb the electronic and chemical properties of Ni ad-atoms, resulting in an inferior ability of Ni with regard to CO methanation [26,27].

Besides Ni-based catalysts, various transition metals have been also tested for ESR, with Co-based catalysts being among the most efficient [34–46]. In particular, Co/Mg/Al hydrotalcites are very active and stable for ESR, due to the formation of highly reactive Co^{2+} species instead of less active metallic cobalt [42–44]. Moreover, Co/CeO_2 catalysts demonstrated excellent ESR activity, ascribed mainly to the high oxygen storage capacity (OSC) of ceria, which suppresses the carbon deposition (e.g., [35,36,41]). In this regard, very active Co-based catalysts can be designed by properly adjusting the local surface structure of Co species by means of support and/or active phase modification [35–46]. For instance, it was found that the addition of Rh as a promoter at small amounts (0.1 wt.%) on 2.0 wt.% Co/CeO_2 catalysts can notably increase the ESR performance [45,46]. Rhodium, through hydrogen spillover phenomena, facilitates the reduction of both cobalt oxides and ceria, which then is reflected on steam reforming performance. The presence of Rh in Co/Ceria catalysts hinders the formation of acetone as well as the build-up of strongly bonded carbide species, leading to improved activity and stability [45,46].

In the light of the above aspects, the present manuscript aims to comparatively explore ESR performance over different CeO_2-supported transition metal (Ni, Fe, Cu, Co) catalysts. The effect of several operation parameters, related to reaction temperature (400–800 °C), time on stream (24 h), S/C feed ratio (0.5, 1.5, 3, 6), and metal loading (15–30 wt.%) on the activity and stability performance is systematically examined. Furthermore, an extensive characterization study—N_2 adsorption-desorption (BET), X-ray diffraction (XRD), Scanning Electron Microscopy (SEM/EDX), X-ray Photoelectron Spectroscopy (XPS), and Temperature Programmed Reduction (H_2-TPR)—was carried out to attain a possible structure-activity relationship. Although recent efforts on ESR are focusing to develop efficient catalysts with low metal contents (e.g., [45,46]), relatively high metal loadings (15–30 wt.%) are employed in the present study, motivated by the potential application of these materials as anodic electrodes in internal reforming ethanol fed SOFCs.

2. Results

2.1. Characterization Studies

2.1.1. Textural Characterization (BET Analysis)

Table 1 presents the textural characteristics (surface area, pore volume, pore diameter) of as prepared catalysts. It is obvious that the addition of transition metals to the ceria carrier has a detrimental effect on the resulted BET area, which, in general, is exacerbated upon increasing the metal content. However, the decrease of BET area upon increasing the cobalt content is not monotonic. The latter can be attributed to the different crystallite size of Co_3O_4 and CeO_2 phases in Co/CeO_2 catalysts, as determined by XRD analysis presented in the sequence. The size of Co_3O_4 is about 3-fold higher than CeO_2 indicating the segregation of cobalt species over the catalyst surface (Table 2). Thus, a significant decrease of bare ceria area (71.5 m^2/g) is expected upon increasing Co loading, due to the blockage of ceria pores. However, this decrease could not be monotonic, since above a certain Co content the formation of large Co_3O_4 particles hampers the dispersion of Co_3O_4 entities into CeO_2 pores and consequently any further decrease of BET area. The same trend was observed upon increasing Cu content in Cu/CeO_2 catalysts [47].

Regarding the M/CeO_2 catalysts with a constant metal loading (20 wt.%), Ni- and Fe-based catalysts possess the higher BET area (~57 m^2/g), while the Cu- and Co-based samples exhibited lower values of surface area, *i.e.*, 44.6 and 33.4 m^2/g, respectively. These variations in the textural characteristics could be related with the different crystallite size of the metal oxides formed in each case, as is discussed later.

Table 1. Textural characteristics of M/CeO_2 (M: Fe, Co, Ni, Cu) catalysts.

Sample	SBET (m^2/g)	Total Pore Volume (cm^3/g)	Average Pore Diameter (nm)
CeO_2	71.5	0.27	15.4
15 wt. % Co/CeO_2	64.2	0.28	17.8
20 wt. % Co/CeO_2	33.4	0.13	16.0
25 wt. % Co/CeO_2	42.2	0.19	18.2
30 wt. % Co/CeO_2	44.9	0.21	18.7
20 wt. % Ni/CeO_2	57.6	0.54	37.7
20 wt. % Cu/CeO_2	44.6	0.15	13.1
20 wt. % Fe/CeO_2	57.0	0.26	18.3

Table 2. Structural characteristics of M/CeO_2 (M: Fe, Ni, Co, Cu) catalysts.

Samples	Phase Detected	Crystallite Size (nm)	Lattice
15 wt.% Co/CeO_2	CeO_2	11.5	Cubic
	Co_3O_4	30.8	Cubic
20 wt.% Co/CeO_2	CeO_2	10.2	Cubic
	Co_3O_4	37.7	Cubic
25 wt.% Co/CeO_2	CeO_2	13.6	Cubic
	Co_3O_4	32.3	Cubic
30 wt.% Co/CeO_2	CeO_2	10.4	Cubic
	Co_3O_4	37.7	Cubic
20 wt.% Fe/CeO_2	CeO_2	10.6	Cubic
	Fe_2O_3	34.1	Rhombohedral
20 wt.% Ni/CeO_2	CeO_2	11.2	Cubic
	NiO	23.2	Cubic
20 wt.% Cu/CeO_2	CeO_2	9.3	Cubic
	CuO	43.5	Monoclinic

2.1.2. Structural Characterization (XRD Analysis)

Figure 1A depicts the XRD spectra of M/CeO_2 catalysts, whereas Figure 1B presents the corresponding spectra of Co-based catalysts of different metal loading. Table 2 lists the phases that were detected for each sample, the corresponding structure, and approximate crystallite size as determined by Scherrer analysis. All metals crystallized in the form of oxides, *i.e.*, iron as Fe_2O_3, cobalt as Co_3O_4, nickel as NiO, and copper as CuO, with their average particle size following the order: CuO > Co_3O_4 > Fe_2O_3 > NiO (Table 2). Regarding CeO_2 crystallites their size increases with the decrease of the corresponding size of the metal oxide phase. Concerning the Co-based catalysts of different metal content, cobalt is again presented in the form of oxide (Co_3O_4), regardless of the Co loading. The crystallite size of CeO_2 remains almost constant upon increasing the Co content. Additionally, the size of Co_3O_4 phase is increased from 30.8 to 37.7 nm with the increment of Co content from 15 to 20 wt.%. However, no further increase was observed for higher Co loadings, confirming the stabilization of BET area values above a certain Co loading.

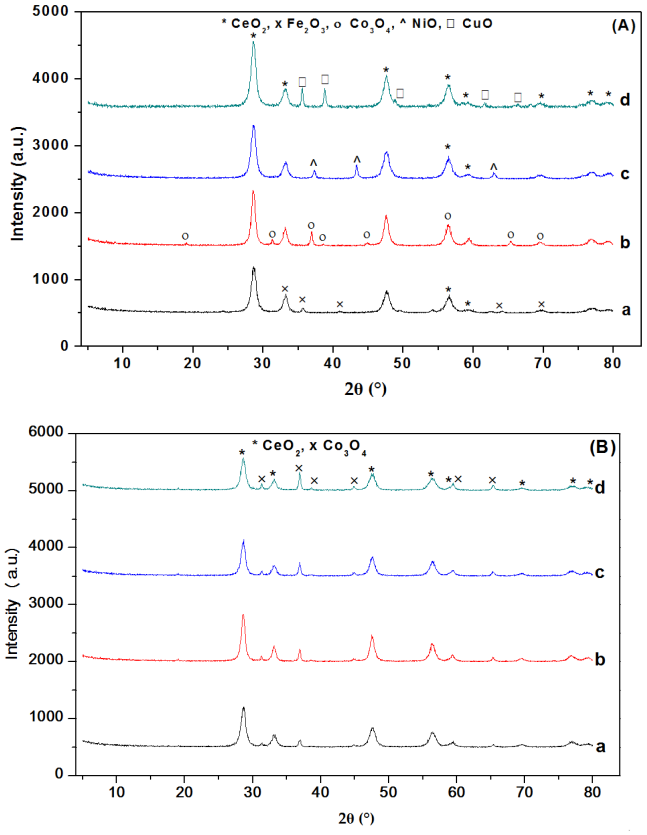

Figure 1. X-ray powder diffraction patterns of 20 wt.% M/CeO_2 catalysts (**A**) where M stands for Fe (a), Co (b), Ni (c) and Cu (d), and of Co/CeO_2 catalysts (**B**) with 15 (a), 20 (b), 25 (c) and 30 wt.% (d) Co loading.

2.1.3. Reducibility Studies (H_2-TPR)

Temperature-programmed reduction (TPR) experiments were performed to gain insight into the role of metal entity on the reducibility of M/CeO_2 catalysts. Figure 2 depicts the TPR profiles of M/CeO_2 catalysts, in terms of hydrogen consumption as a function of temperature.

In the Cu/CeO_2 sample the overlapping peaks at 100–300 °C temperature interval are assigned to Cu oxide species reduction along with the surface oxygen reduction [48–52]. Specifically, the peak at 133 °C is attributed to the reduction of Cu ions in close proximity to CeO_2, while, the features at 215 °C and 267 °C are assigned to Cu entities not closely associated with ceria [52].

In the Co/CeO_2 sample no obvious peaks were detected at temperatures lower than 300 °C, denoting that Co species, in contrast to Cu, are more difficult to reduce. The Co/CeO_2 reduction profile was comprised of several overlapping features in the *ca.* 300–400 °C temperature range. These peaks are related to the reduction of surface oxygen groups along with the stepwise reduction of Co oxides to metallic cobalt [53].

Ni/CeO_2 catalysts mainly exhibit two reduction peaks at 231 and 330 °C. The peak at 231 °C is attributed to adsorbed surface oxygen reduction, while the peak at 330 °C to the reduction of the bulk NiO and surface CeO_2 [54–57].

Concerning the reduction profile of Fe/CeO_2 sample, it has been widely recognized that hematite (Fe_2O_3) reduction to metallic iron (Fe^0) takes place through the formation of magnetite (Fe_3O_4) and wustite (FeO). Wustite is metastable and disproportionates into magnetite and metallic iron ($4FeO \rightarrow Fe_3O_4 + Fe$) below 620 °C [58]. Commonly, bare iron oxide shows overlapping features at *ca.* 300–800 °C, corresponding to the stepwise reduction of hematite to metallic iron [58–60]. The Fe/CeO_2 sample exhibits in addition a main peak at 296 °C, which can be attributed to surface oxygen reduction

as well as to the facilitation of the stepwise reduction of Fe oxides to metallic iron. Based on the main hydrogen TPR peaks, the following order of reducibility was recorded: Cu/CeO_2 > Fe/CeO_2 > Ni/CeO_2 > Co/CeO_2.

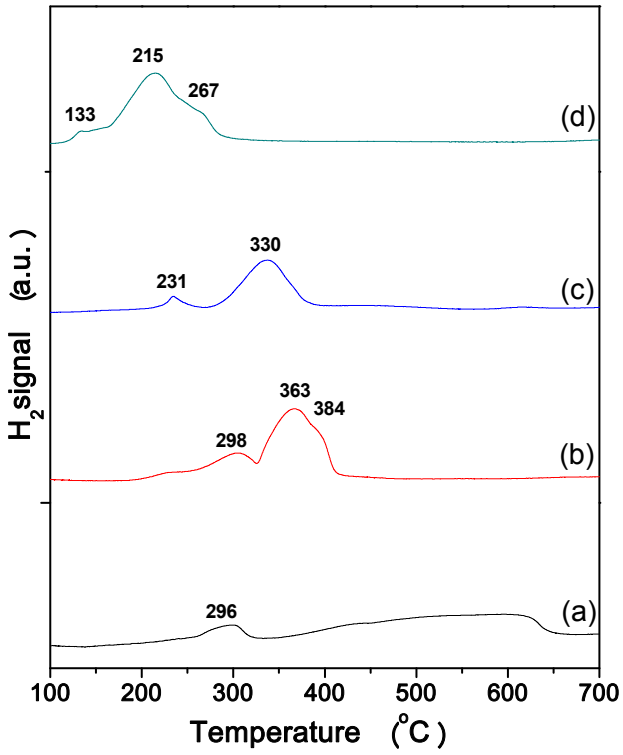

Figure 2. Temperature programmed reduction profiles of 20 wt.% Fe (a), Co (b), Ni (c) and Cu (d) catalysts supported on CeO_2.

2.1.4. Surface Characterization (XPS Analysis)

XPS measurements were carried out next to obtain insights into the elemental oxidation states and surface composition. Figure 3 depicts the XPS spectra in the 2p region of Fe, Co, Ni, and Cu catalysts supported on ceria. In the case of the Fe/CeO_2 sample, peaks in the region of 709–713 eV with satellites at *ca.* 725 eV appear. Curve-fitting revealed the contribution of Fe^{2+} and Fe^{3+} ions at 709–711 eV and 711–713 eV, respectively [61,62]. The presence of a certain amount of Fe^{2+} ions probably implies the co-existence of Fe_2O_3 (as indicated by XRD) with lower valence iron oxides (FeO/Fe_3O_4). The Co 2p spectrum of Co/CeO_2 catalyst is characterized by a main peak at 780.6 eV accompanied by a low intensity satellite and a spin-orbit doublet $Co2p_{1/2}$-$Co2p_{3/2}$ of 15.2 eV. These characteristics point to the formation of Co^{3+} species in Co_3O_4-like phase [54]. The $Ni2p_{3/2}$ can be analyzed into two components corresponding to different Ni chemical states. The peak at *ca.* 854 eV is usually assigned to NiO, whereas the higher BE peak at 855–856 eV to Ni bonded with OH groups, *i.e.*, $Ni(OH)_2$ and/or NiOOH [63,64]. It should be noted, however, the difficulty of unambiguously assigning the different chemical states of Ni oxides due to the complexity of Ni 2p spectra arising from multiplet splitting, shake-up satellites, and plasmon loss structures [65]. In any case the majority of Ni species seems to be related with NiO in accordance with the XRD findings. The spectrum of the Cu/CeO_2 sample is characterized by a Cu $2p_{3/2}$ band at 933.8 eV and shake-up satellites at *ca.* 944.0 eV, typical characteristics of Cu^{2+} species in CuO-like phase [20,48,66–70]. The above assignments are in line with the XRD findings, which revealed the formation of the corresponding metal oxides in M/CeO_2 samples (Table 2).

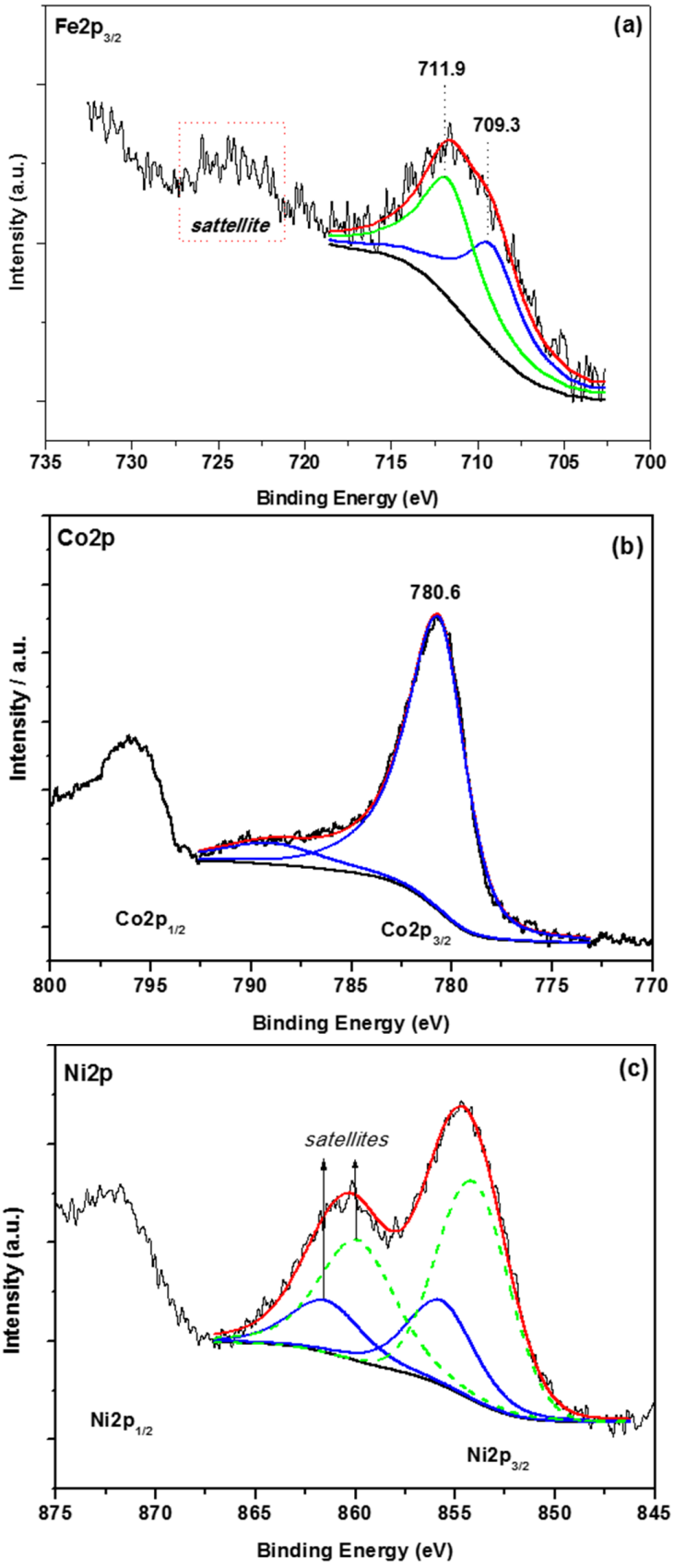

Figure 3. *Cont.*

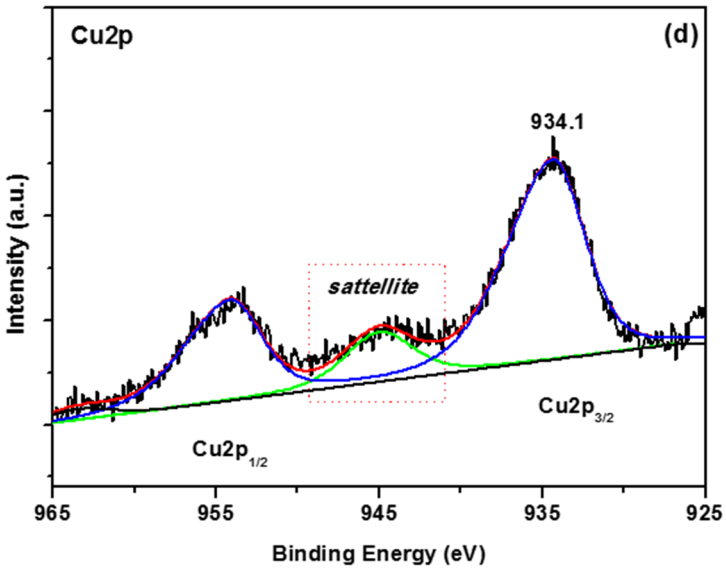

Figure 3. Core level 2p spectra of 20 wt.% Fe (**a**); Co (**b**); Ni (**c**) and Cu (**d**) catalysts supported on CeO_2.

Figure 4 depicts the O1s spectra of M/CeO_2 samples. Curve-fitting, based on a mixture of Lorentzian and Gaussian curves, revealed three components. The low binding energy peak (O_I) at ~529 eV can be ascribed to lattice oxygen, the intermediate peak (O_{II}) at ~531 eV to surface O, OH groups and oxygen vacancies and the high energy band (O_{III}) at ~534 eV to adsorbed water [68,71,72]. In the case of Ni/CeO_2 the low BE peak at *ca.* 527 eV could be due to the differential charging of the oxide. Based on the area of O_I, O_{II} and O_{III} envelopes, a relative comparison between the M/CeO_2 samples could be obtained (Table 3). It is evident that the ratio between the lattice oxygen to the sum of surface oxygen species notably changes with the metal type. Co/CeO_2 catalysts possess the highest amount of O_I species (70%), which are related to lattice oxygen in ceria and cobalt oxides. These differences in the population of surface oxygen species are expected to affect the redox reactions between the gaseous reactants and solid carbonaceous deposits with lattice oxygen ions, as is discussed in the sequence.

Table 3. Percentage of surface oxygen species on M/CeO_2 catalysts.

Sample	%		
	O_I	O_{II}	O_{III}
Fe/CeO_2	48	45	7
Co/CeO_2	70	24	6
Ni/CeO_2	46	54	-
Cu/CeO_2	38	55	7

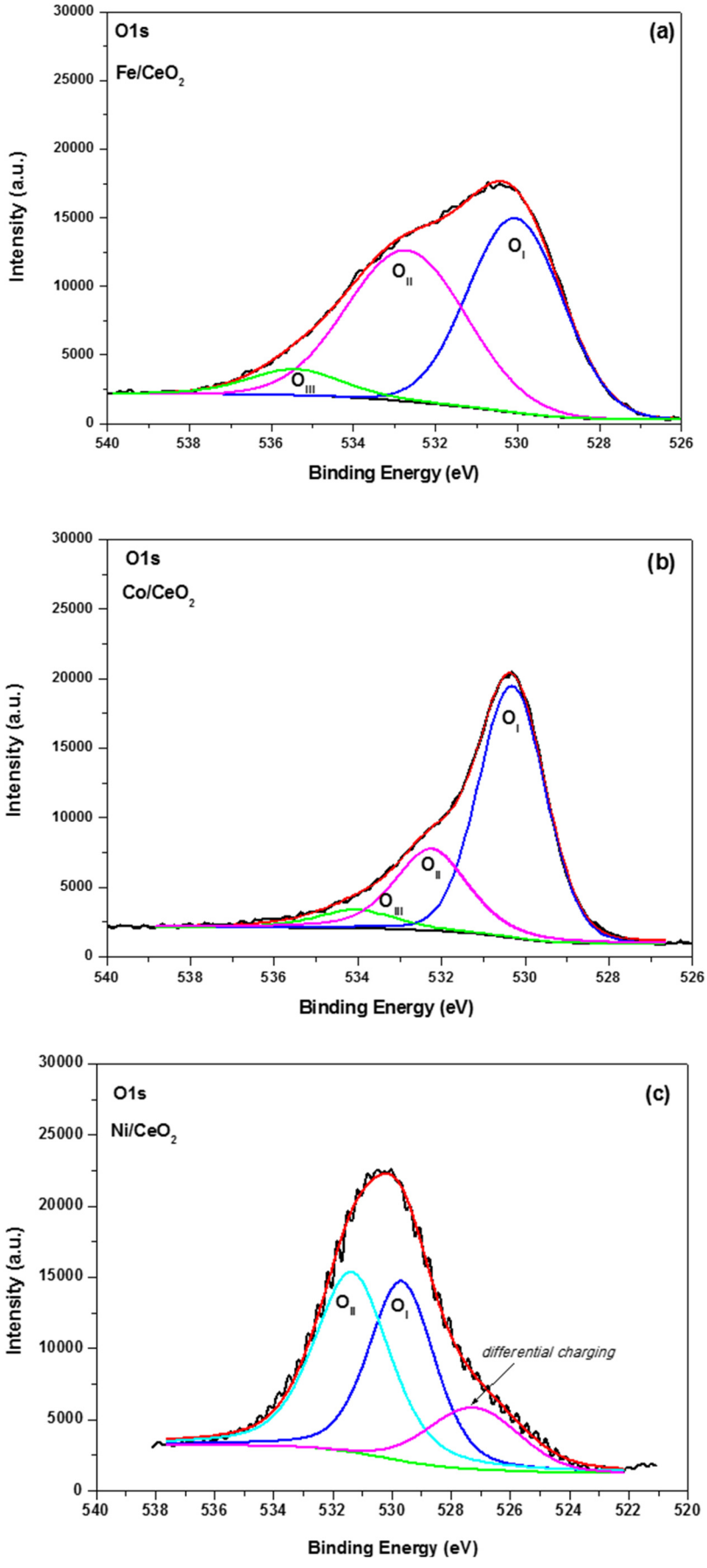

Figure 4. *Cont.*

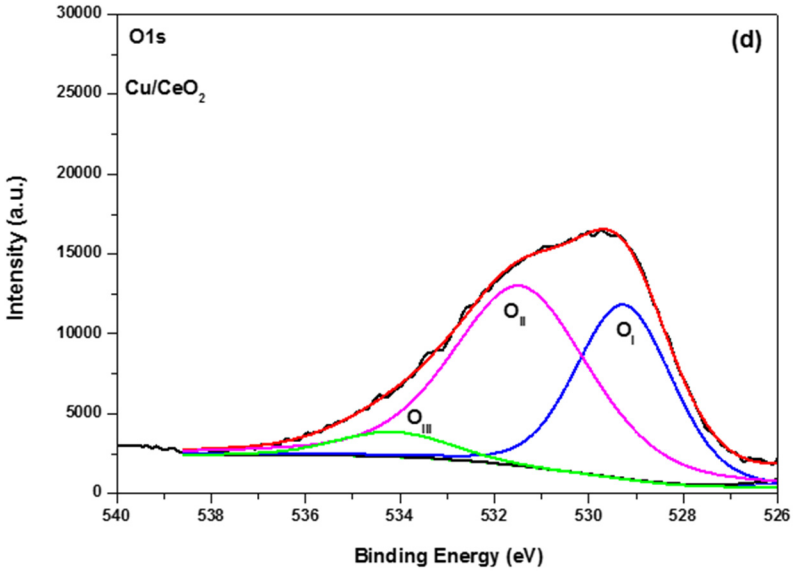

Figure 4. O1s spectra of Fe (**a**); Co (**b**); Ni (**c**) and Cu (**d**) catalysts supported on CeO_2.

The surface composition of M/CeO_2 samples obtained by XPS analysis, along with the bulk atomic concentrations (at. %), is presented in Table 4. Comparison of the XPS and nominal values of transition metal (Fe, Co, Ni, Cu) atomic concentrations reveals a decrease in metal surface species for all samples. These findings can be understood to a good extent considering surface characterization studies over Co-Ce binary oxides [53], where it was demonstrated the impoverishment of catalyst surface in Co species during the calcination procedure. The latter has been mainly attributed to the low surface energy of cobalt compared to ceria, resulted in a localization of ceria on the outer surface. In a similar manner, it has been revealed that the surface concentration of metal ions (such as Ni and Co) supported on ceria-based materials can be notably decreased due to the incorporation of metal ions into the support lattice [73–75]. This particular configuration, involving the coexistence of metal ions in the outer surface and inside the support structure, could largely favor the oxygen mobility, with large consequences in the catalytic activity (e.g., [75]).

Table 4. Bulk and surface—X-ray Photoelectron Spectroscopy (XPS)—atomic concentrations (at%) for 20 wt.% M/CeO_2 catalysts.

Samples	XPS [a]				Nominal [b]			
	M	Ce	O	M/Ce	M	Ce	O	M/Ce
Fe/CeO_2	7.7	29.6	62.7	0.26	15.6	20.3	64.1	0.77
Co/CeO_2	11.0	25.5	63.5	0.43	15.5	21.3	63.2	0.73
Ni/CeO_2	15.4	23.5	61.1	0.65	16.4	22.4	61.2	0.73
Cu/CeO_2	8.2	34.0	57.8	0.24	15.5	23.0	61.5	0.68

[a] estimated from XPS spectra; [b] calculated from the nominal catalyst composition, assuming that M is oxidized to M_xO_y during the preparation procedure, as indicated by XRD analysis.

2.2. *Catalytic Activity Studies*

2.2.1. Effect of Metal Entity on Steam Reforming Performance

Ethanol Steam Reforming (ESR) is a multi-molecular reaction involving several pathways producing hydrogen, CO, CO_2 and numerous by-products, such as methane, ethylene, acetaldehyde, acetone, coke, *etc.* [76]. The simplified reaction network, presented in Figure 5, can be considered for the different product distribution during ESR [77,78]. This mainly involves apart from the ESR

(Equation (1)) and water gas shift (Equation (2)) reactions, the ethanol decomposition (Equation (3)), ethanol dehydrogenation (Equation (4)), acetaldehyde decarbonylation (Equation (5)), acetone formation via acetaldehyde condensation, followed by decarboxylation (Equation (6)), ethanol dehydration (Equation (7)), methanation (Equation (8)), and carbon deposition (Equation (9)) reactions:

$$C_2H_5OH_{(g)} \rightarrow CO_{(g)} + CH_{4(g)} + H_{2(g)}, \Delta H^0_{298} = 49\,kJ/mol \quad (3)$$

$$C_2H_5OH_{(g)} \rightarrow H_{2(g)} + CH_3CHO_{(g)}, \Delta H^0_{298} = 69\,kJ/mol \quad (4)$$

$$CH_3CHO_{(g)} \rightarrow CH_{4(g)} + CO_{(g)}, \Delta H^0_{298} = -19\,kJ/mol \quad (5)$$

$$CH_3CHO_{(g)} \rightarrow 1/2CH_3COCH_{3(g)} + 1/2CO_{(g)} + 1/2H_{2(g)}, \Delta H^0_{298} = 2.8\,kJ/mol \quad (6)$$

$$C_2H_5OH_{(g)} \rightarrow C_2H_{4(g)} + H_2O_{(g)}, \Delta H^0_{298} = 45\,kJ/mol \quad (7)$$

$$CO_{(g)} + 3H_{2(g)} \leftrightarrow CH_{4(g)} + H_2O_{(g)}, \Delta H^0_{298} = -205\,kJ/mol \quad (8)$$

$$2CO_{(g)} \rightarrow C_{(s)} + CO_{2(g)}, \Delta H^0_{298} = -171.5\,kJ/mol \quad (9)$$

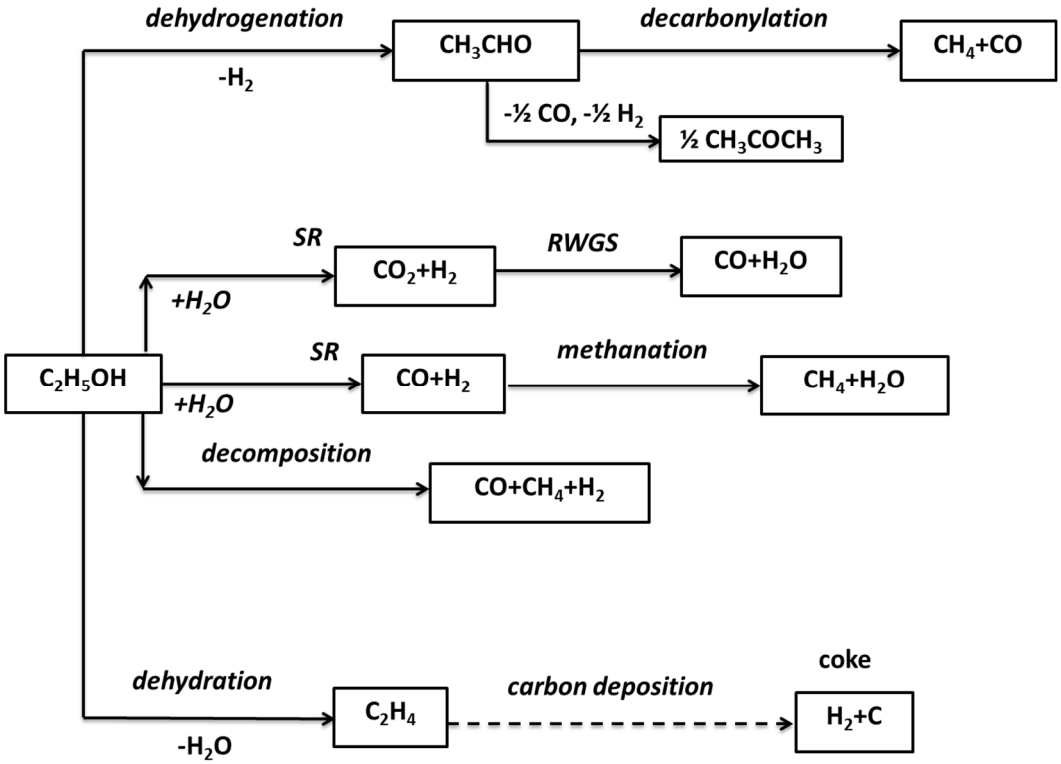

Figure 5. Schematic representation of the reaction network in the ethanol steam reforming (ESR) process.

Figure 6 depicts the effect of temperature (400–800 °C) on ethanol conversion and product selectivity during the ESR over M/CeO_2 catalysts, at a constant S/C feed ratio of 3. The reforming process resulted mainly to H_2, CO, CO_2, and CH_4. Minor quantities of C_2H_4, C_2H_6, and traces of CH_3CHO and CH_3COCH_3 are also observed. The H_2 selectivity follows, in general, a downward shift with increasing temperature, in contrast to CO selectivity. The particular high hydrogen selectivities at lower temperatures (400–500 °C) in the case of Fe-, Co- and Cu-based samples, which exceed the expected theoretical values from reaction stoichiometry, maybe due to the thermal decomposition and/or parallel reactions taking place at low temperatures. The latter keeps in step with the extended carbon formation at low temperatures, as will be discussed in the sequence. The selectivity towards

CO_2 and CH_4 decreases up to 600 °C and then gradually level-off until 800 °C. The variation of H_2, CO, CO_2, and CH_4 selectivity upon increasing temperature can be realized by taking into account the different reactions involved in ESR (Figure 5). At low temperatures the WGS reaction (Equation (2)) is favored, increasing the selectivity towards H_2 and CO_2. In contrast, at high temperatures the reverse WGS reaction enhances the production of CO and H_2O at the expense of H_2 and CO_2. The decrease of CH_4 formation at higher temperatures may be ascribed to its reforming to CO and H_2 [32].

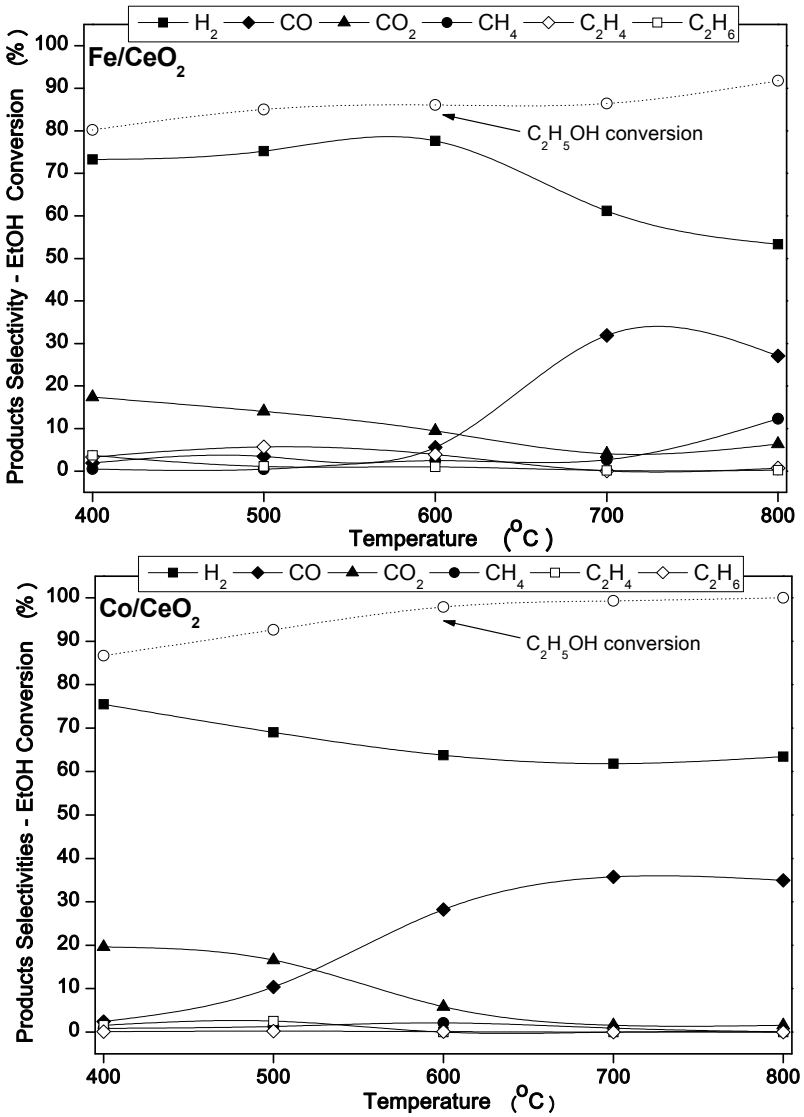

Figure 6. *Cont.*

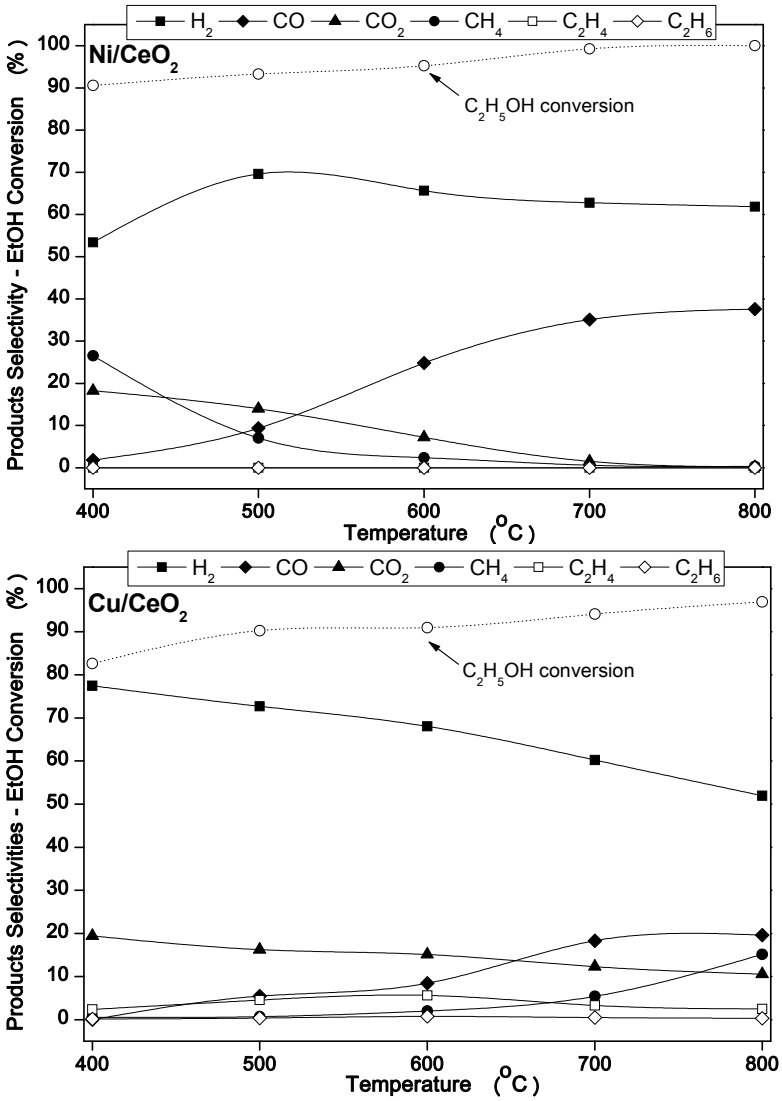

Figure 6. Effect of temperature on product selectivity and C_2H_5OH conversion over M/CeO_2 catalysts. Reaction conditions: S/C = 3, m_{cat} = 250 mg, F_T = 150 cm^3/min.

The impact of catalyst type (Fe, Co, Ni, Cu) and temperature on product distribution is more evident in Figure 7, which comparatively depicts the major product yield at 400, 600 and 800 °C. For comparison purposes the corresponding results over bare CeO_2 are also depicted. The superior performance of M/CeO_2 catalysts compared to bare CeO_2 is clearly shown. The latter implies the pronounced effect of transition metal and/or metal-support interfacial sites on ethanol steam reforming, as discussed in the sequence. At 400 °C the best performance, in terms of H_2 yield, is achieved by Co- and Cu-based catalysts both exhibiting a H_2 yield of ~66%. Fe- and Ni-based catalysts demonstrated lower H_2 yields of 59% and 48%, respectively. Ni/CeO_2 catalysts display very high CH_4 yield (24%), compared to all other M/CeO_2 catalysts (~0.4%). This can be attributed to the acetaldehyde decarbonylation to CH_4 (Equation (5)) over Ni sites at low temperatures [77,79–83]. At 600 °C, the Co-, Ni-, and Cu-based catalysts demonstrated a similar H_2 yield of ~62%, with Fe/CeO_2 catalyst exhibiting a slightly better yield (~67%). It is worth mentioning that at 600 °C CO formation is in general favored at the expense of CO_2, probably implying participation of the reverse WGS reaction on the ESR reaction network (Figure 5). At 800 °C the Co- and Ni-based catalysts showed H_2 yields of 65% and 62%, respectively, followed by a CO yield of 35% and 38%. Therefore, in these catalysts, the ESR reaction leads almost exclusively to H_2 and CO. In contrast, the Fe- and Cu-based catalysts as well

as the bare CeO_2 exhibited significantly lower syngas yields and higher amounts of CH_4, implying an inferior reforming performance at high reaction temperatures.

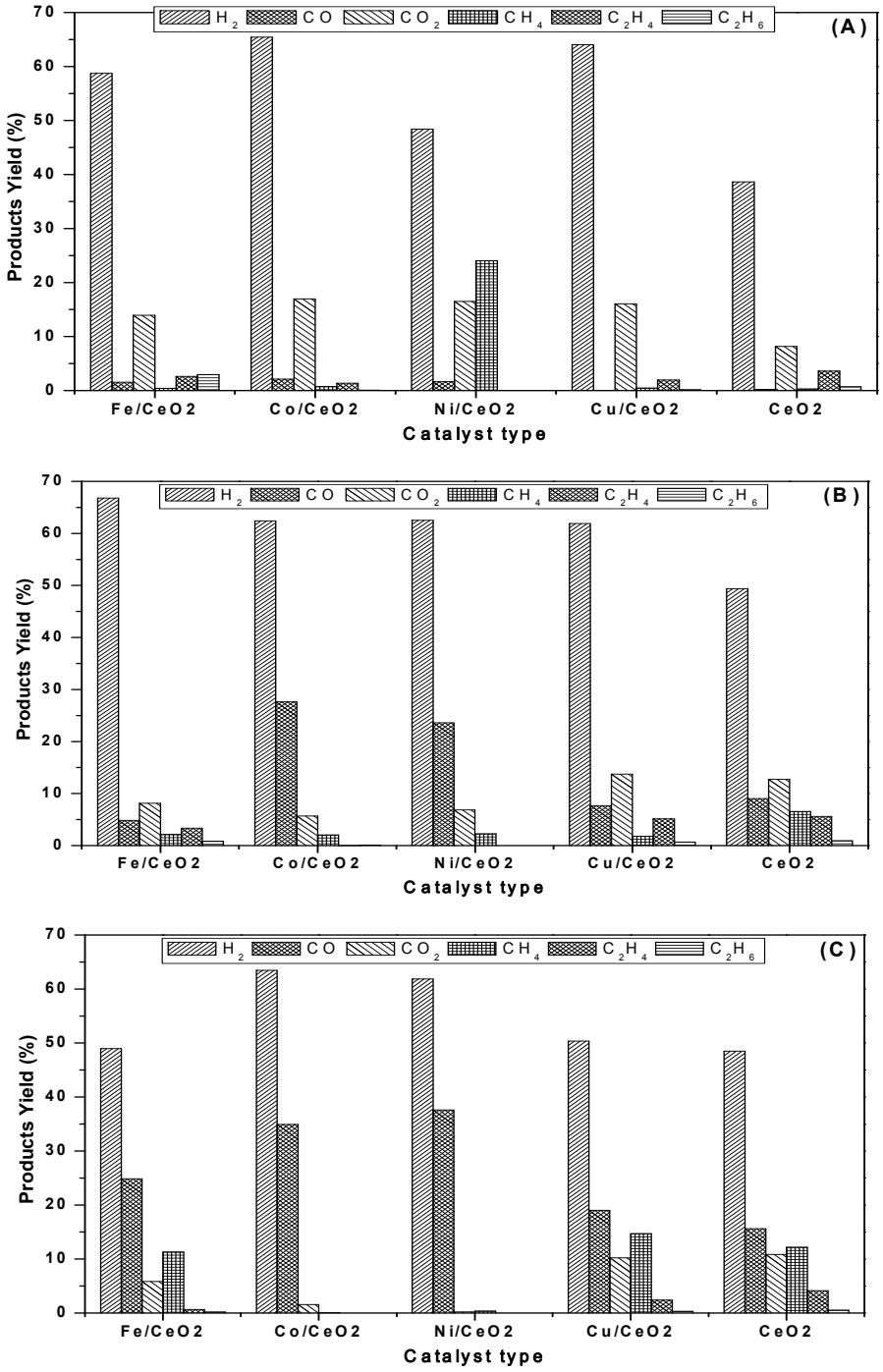

Figure 7. Effect of metal type on major product yield at 400 °C (**A**); 600 °C (**B**) and 800 °C (**C**). Reaction conditions: S/C = 3, m_{cat} =250 mg, F_T = 150 cm^3/min.

2.2.2. Effect of Metal Loading

Figure 8 depicts the effect of Co loading on the main products yield at 400, 600 ,and 800 °C. It is evident that in the absence of metal (bare CeO_2), the yields toward the reformate products (CO and H_2) are much lower compared to the corresponding ones over Co/CeO_2 catalysts. At 400 °C the

optimum H_2 yield (~66%) is obtained for 20 wt.% metal loading, whereas at higher temperatures both the absolute products yields and product distribution are almost independent of the metal loading (0–30 wt.%).

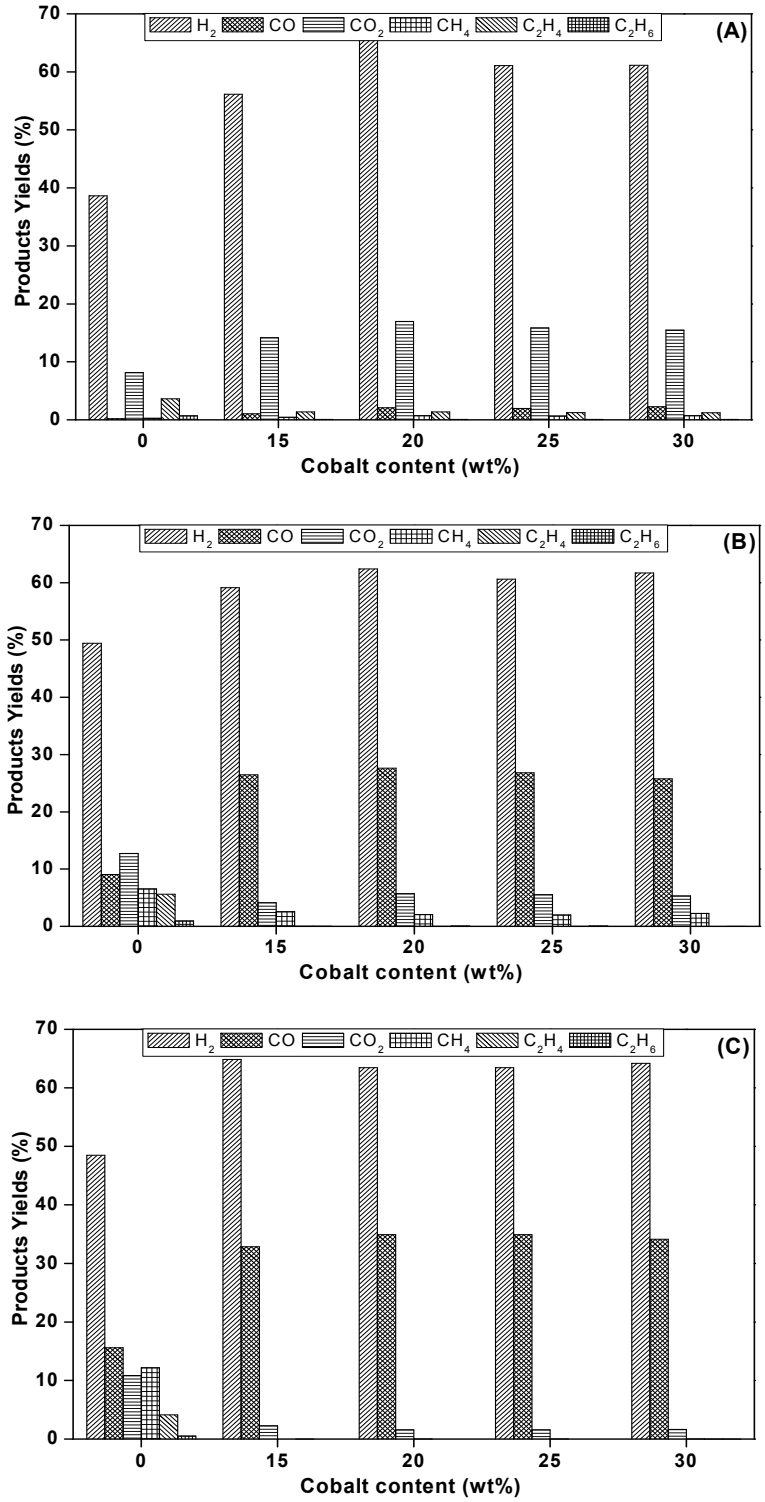

Figure 8. Effect of Co loading in Co/CeO_2 catalysts on products yield at 400 °C (**A**); 600 °C (**B**) and 800 °C (**C**). Reaction conditions: S/C = 3, m_{cat} = 250 mg, F_T = 150 cm^3/min.

2.2.3. Effect of S/C Ratio

Figure 9 presents the effect of S/C (0.5, 1.5, 3, 6) feed ratio on the major product yield achieved over the 20 wt.% Co/CeO_2 catalyst. At low temperatures, *i.e.*, at 400 °C, the optimum performance is obtained for S/C reactants ratio of 3 (~66%), whereas for temperatures higher than 400 °C the H_2 yield is maximized for a S/C feed ratio of 6. At 800 °C the yield toward H_2 is equal to 77% for a S/C ratio of 6, as compared to approximately 63% for lower S/C ratios. However, it is worth noticing, that for a S/C ratio of 3 the largest fuel production was experienced, *i.e.*, sum of H_2 and CO, as the yield with regard to CO_2 and hydrocarbons is essentially negligible. Therefore, the S/C ratio equal to 3 can be regarded as optimal, in terms of ethanol energy exploitation.

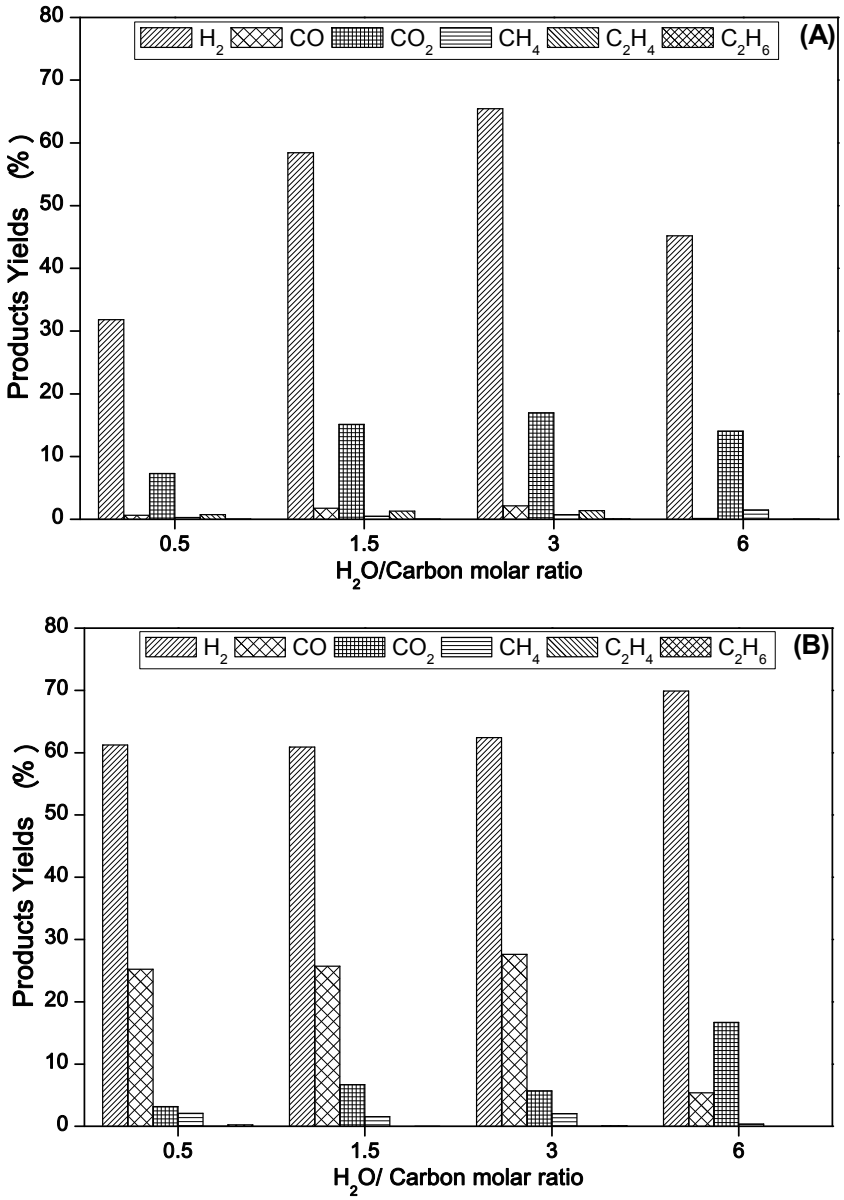

Figure 9. *Cont.*

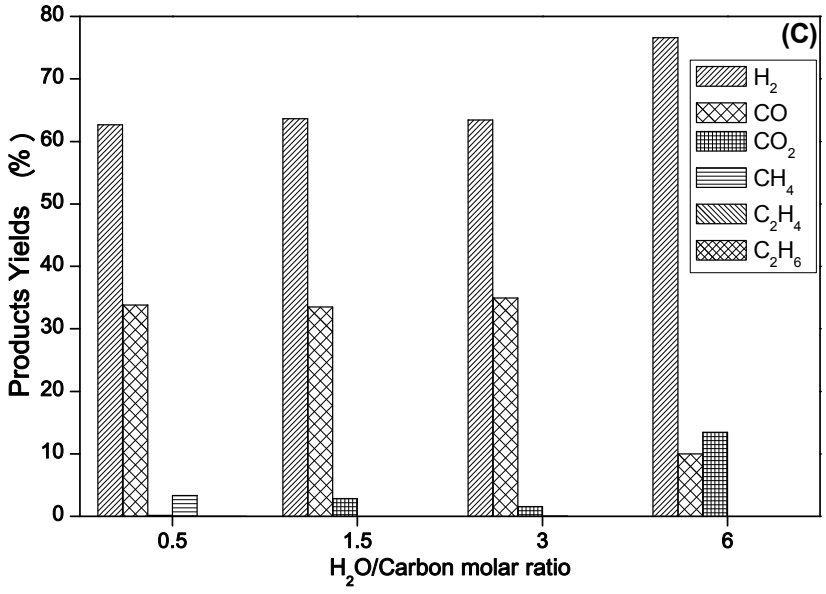

Figure 9. Effect of H_2O/Carbon (S/C) feed molar ratio on product yield at 400 °C (**A**); 600 °C (**B**) and 800 °C (**C**) over 20 wt.% Co/CeO_2 catalyst. Reaction conditions: m_{cat} = 250 mg, F_T = 150 cm^3/min.

2.2.4. Stability Experiments

Short-term (24 h) stability experiments were then carried out over Co-, Ni-, Fe- and Cu-CeO_2 catalysts to assess the catalyst life time characteristics. Stability experiments were performed at low (400 °C), intermediate (600 °C) and high (800 °C) temperatures to reveal the effect of temperature on stability performance. Figure 10 depicts the H_2 production rate at 400 °C (A), 600 °C (B) and 800 °C (C) *versus* time on stream (TOS) at a steam-to-carbon (S/C) ratio equal to 3. In these experiments the catalyst was first exposed to pure He up to the desired temperature, and then the standard feed mixture was introduced into the reactor.

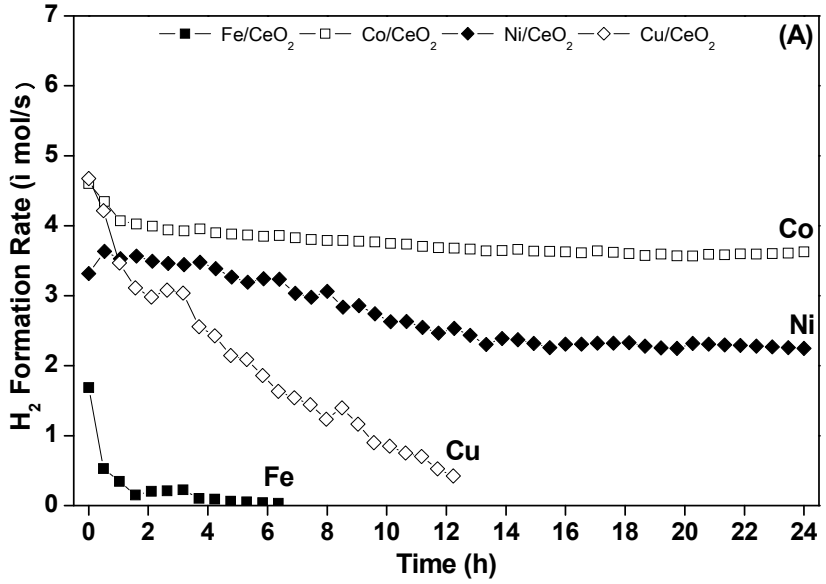

Figure 10. *Cont.*

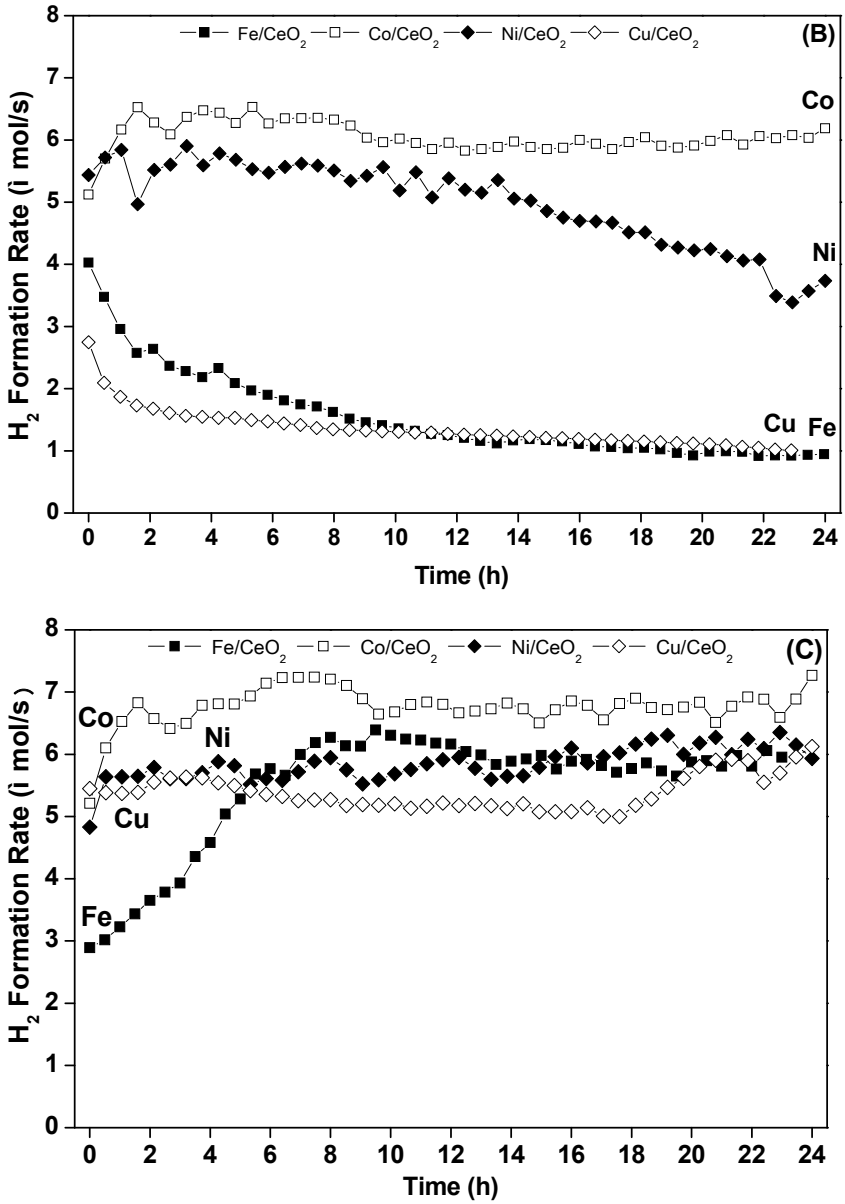

Figure 10. Stability performance of M/CeO_2 catalysts (M: Fe, Co, Ni, Cu) at 400 °C (**A**); 600 °C (**B**) and 800 °C (**C**) during ESR. Reaction conditions: S/C=3, m_{cat} = 250 mg, F_T = 150 cm^3/min.

The superiority of Co/CeO_2 catalysts in terms of H_2 production and stability is obvious. Co-based catalysts demonstrated an excellent stability performance at 600 and 800 °C whereas a slight degradation was observed at 400 °C. At low temperatures (400 °C) the formation rate of hydrogen was gradually decreased over Ni/CeO_2 catalysts during the first 13 h, remaining then stable. A more rapid deactivation was obtained with Cu- and Fe-based catalysts, which were totally deactivated after about 12 and 4 h, respectively. A similar picture was recorded at intermediate temperatures (Figure 10B), although in this case the deactivation was milder. Ni/CeO_2 catalysts were stable in the first 14 h, declined then steadily. Cu- and Fe-based catalysts followed a downgrade trend in the first 10 h, stabilized then at very low levels. In contrast, at high temperatures, *i.e.*, 800 °C (Figure 10C), all catalysts demonstrated an adequate stability performance throughout the period of 24 h.

3. Discussion

The present findings clearly demonstrated the superior steam reforming performance of Co/CeO_2 catalysts, in terms of H_2 production and stability, in the examined temperature range of 400–800 °C. In contrast all other catalysts (Fe-, Ni-, Cu-CeO_2) exhibited satisfactory stability only at high temperatures (800 °C), whereas at low and intermediate temperatures a gradual deactivation was observed, being more intense for Cu- and Fe-based catalysts. The optimum performance of high metal loading Co-based catalysts, compared to conventional Ni-based catalyst, should be also emphasized. The latter is of major importance with regard to the direct utilization of ethanol in SOFCs, where highly active, conductive and robust electro-catalysts are required [84].

To better understand the influence of temperature and catalyst nature on stability performance indicative morphological studies (SEM/EDS) were carried out over the fast deactivated Cu/CeO_2 catalysts and very stable Co/CeO_2 catalysts (not shown for brevity's sake). In general, a significant amount of carbon was detected over Cu/CeO_2 exposed for 24 h to reaction conditions at 400 °C, which, however, decreased at 600 °C and was almost eliminated at 800 °C. To be specific, a small amount of deposited carbon, mostly in the form of carbon fibers, was identified at elevated temperatures. Moreover, no significant changes in the particle size were recorded upon temperature increase.

Given that the Cu/CeO_2 catalyst maintains its activity at 800 °C (Figure 10C) it could be argued that neither catalyst particle sintering nor the formation of carbon fibers could affect the catalysts' stability at high temperatures. In this regard, it has been shown that filamentous carbon does not directly lead to the poisoning of CeO_2-based catalysts in ESR, although it delaminates metal particles from the support; amorphous carbon tends to block active sites leading to deactivation [85]. Therefore, the deactivation of Cu/CeO_2 catalysts at low (400 °C), and to a lesser extent at intermediate (600 °C) temperatures, can be mainly ascribed to amorphous carbon deposition. The improved stability performance at 600 °C, compared to 400 °C, can be attributed to the facile gasification of carbonaceous deposits at elevated temperatures [85–87].

Similar conclusions, in relation to the impact of reaction temperature on the carbon deposition and particle size of Co/CeO_2 catalysts were obtained by means of SEM/EDS analysis. The particle size remained practically unaffected by temperature increase to 600 °C, whereas it was slightly increased after reaction at 800 °C. Amorphous carbon was revealed by EDS analysis and elemental mapping for spent Co/CeO_2 at 400 °C, although at a relatively lesser amount compared to Cu/CeO_2. Carbon was also identified at 600 °C, but at a significantly lower amount to that observed at 400 °C. At higher temperature of 800 °C the carbon was almost absent.

In the light of the above results, it could be stated that Co/CeO_2 catalyst displayed the optimum reforming performance in terms of H_2 yield and life-time stability. In contrast, an inferior performance was obtained over Ni-, Cu- and Fe-based catalysts. In a similar manner, it was found that neither Cu nor Ni supported on ZnO catalysts were stable in ESR conditions [24]. On Cu/ZnO the dehydrogenation of ethanol into acetaldehyde was favored, whereas on Ni/ZnO the decomposition of ethanol to CH_4 and CO_x took place.

The present findings can be mainly interpreted by taking into account the surface and redox properties of transition metal-based catalysts. TPR studies revealed the lower reducibility of Co/CeO_2 catalyst amongst the investigated samples. The latter, could be possibly related to the strong metal-support interactions, maintaining the Co species in an oxidized state ($Co^{\delta+}$ species). This factor could be considered responsible for the adequate ESR performance of Co/CeO_2 catalysts, in agreement with relevant literature studies [42–44,88–91].

On the other hand, although Cu-based materials are highly reducible under mild conditions, they are almost inactive toward reforming reactions, leading mainly to ethanol dehydrogenation. In this regard, it has been reported that the over-reduction of CeO_2-based materials under H_2-rich environments, can lead to the blockage of the redox mechanism involved in ESR and the carbon gasification reaction network [92–94].

In addition, the high concentration of lattice oxygen in Co/CeO_2, as compared to Fe-, Cu- and $Ni-CeO_2$ catalysts, can be further considered for their superior ESR performance. To this end, the key role of oxygen availability in both H_2 yield and stability of Co-based catalysts has been revealed [36]; the gas-solid interactions between the adsorbed hydrocarbon species (C_nH_m) and the surface oxygen groups (O_x) can facilitate hydrocarbon species gasification instead of their decomposition to carbon.

The inhibition of carbon deposition by gas-solid interactions between hydrocarbons and lattice oxygen has been already demonstrated in several catalytic systems [95–98]. In this regard, isotopic tracer and nuclear reaction analysis (NRA) clearly suggested that methane is selectively oxidized by lattice oxygen ions to produce carbon monoxide during the catalytic partial oxidation (CPOX) of methane to synthesis gas on $Rh/Ce_{0.56}Zr_{0.44}O_{2-x}$ catalysts [97].

Based on the above aspects it can be stated that the intrinsic reactivity of Co entities, along with the strong metal-support interactions in Co/CeO_2 composites, maybe accounted for the high oxidation degree of cobalt entities, as well as for their lower reducibility under reaction conditions. Furthermore, the high concentration of lattice oxygen in the Co/CeO_2 catalyst can be further regarded for the inhibition of carbon deposition through the gas-solid interactions between the adsorbed hydrocarbon species and the lattice oxygen. These factors could be considered equally crucial for the transformation of the deposited carbonaceous species into gaseous products during the stream reforming process.

The present results are in agreement with those obtained over Cu- and Co-based catalysts during ethanol [90] or iso-octane [48,93] steam reforming. Highly reducible Cu-based catalysts are almost inactive for ESR, leading mainly to ethanol dehydrogenation [90]. In contrast, Co/SiO_2 catalysts demonstrated superior reforming performance, despite their limited reducibility at low temperatures due to the strong metal-support interactions [90]. Along the same lines, it has been demonstrated that the oxygen storage capacity of the support can greatly affect the reforming performance of Co-based catalysts by promoting the gasification of carbon deposits [88,91]. To this end, the superior ESR performance of Co/CeO_2 catalysts as compared to ZrO_2- or Al_2O_3-based samples has been ascribed to the abundance of redox sites on the catalyst surface [36,40,41]. More specifically, it has been clearly revealed by means of steady-state reaction experiments coupled with post-reaction characterization techniques that the high oxygen mobility in Co/CeO_2 samples—linked with the high oxygen storage capacity (OSC) of ceria—not only suppresses the carbon deposition, but also allows delivery of oxygen to ethoxy species, thus promoting the complete oxidation of carbon to CO_2 [36].

In the light of the above analysis, it is evident that in order to fully understand the complex and dynamic ESR mechanism of ceria-based transition metal catalysts, it is essential to know the local surface structure and chemistry of active entities under real "working" conditions. This requires the combination of advanced *ex situ* characterization studies with *in situ* operando measurements. In this regard, the key role of metal-ceria interactions on the ESR performance, has been verified by combining *in situ* and *ex situ* characterization techniques [25,41].

4. Materials and Methods

4.1. Materials Synthesis

A series of CeO_2 supported transition metal catalysts (Fe, Co, Ni, Cu) were synthesized using the incipient wet impregnation method. Initially, the bare CeO_2 was prepared by diluting CeO_2 precursor salt ($Ce(NO_3)_3 \cdot 6H_2O$, Sigma Aldrich, Taufkirchen, Germany) in double distilled water. The whole contents were heated and stirred until the evaporation of water. The resulted sample was dried at 100 °C for 16 h and then calcined at 600 °C for 2 h (heating rate: 5 °C/min). The ceria-based catalysts were then prepared via the impregnation of calcined ceria in an aqueous metal (Fe, Co, Ni, Cu) solution, employing the corresponding nitrate salts (Sigma Aldrich, Taufkirchen, Germany) as precursors, at the appropriate concentration so as to yield 20 wt.% metal loading. To explore the impact of metal loading a series of cobalt-based catalysts with metal contents of 15, 20, 25 and 30 wt.% were also prepared

following the same synthesis route. The resulted solutions were heated at first under stirring, then dried overnight at 120 °C and calcined at 600 °C for 2 h.

4.2. Characterization Studies

4.2.1. Textural Characterization (BET)

The textural characteristics of as prepared composites were determined by N_2 adsorption/desorption isotherms at 77 K, employing the multipoint BET analysis in a Tristar Micromeritics 3000 flow apparatus. BET area was measured according to the Brunauer-Emmett-Teller (BET) method at the relative pressure in the range of 0.005–0.99. The total pore volume was estimated by the nitrogen volume at the highest relative pressure. The Barret-Joyner-Halenda (BJH) method was employed to obtain the average pore diameter. Prior to measurements the catalysts were degassed at 250 °C for 16 h.

4.2.2. Structural Characterization

The crystalline structure was determined using the X-ray powder diffraction (XRD) method. A Siemens D 500 diffractometer was employed for the XRD measurements with a Cu Kα radiation (λ = 0.154 nm) operated at 40 kV and 30 mA. Diffractograms were collected in the 2θ = 10°–80° range at a scanning rate of 0.04° over 2 s. The DIFFRAC plus Basic data evaluation software was employed to identify the diffraction peaks and through the Scherrer equation to calculate the crystallite sizes of the detected phases within an experimental error of 10%.

4.2.3. Morphological Characterization

The morphology of fresh and spent catalysts was investigated by scanning electron microscopy (SEM) using a JEOL 6300 microscope, coupled with EDX (Oxford Link ISIS-2000) for the determination of local elemental composition.

4.2.4. Redox Characterization (H_2-TPR)

TPR studies were elaborated in a flow system assembled with a quadrupole mass spectrometer (Omnistar, Balzers). The TPR tests were carried out in a quartz micro-reactor loaded with *ca.* 100 mg of catalyst. Typically, ~100 mg of the material is placed in the reactor and heated to 1000 °C with a heating rate of 10 °C/min under 5% H_2/He flow (50 cm^3/min). All samples were heated at 600 °C for 1 h under 5% O_2/He flow and then cooled down to room temperature, prior to the TPR measurements.

4.2.5. Surface Characterization (XPS)

The photoemission experiments were performed in an ultrahigh vacuum system (UHV), comprised of a fast entry specimen assembly, a sample preparation chamber and an analysis chamber. The base pressure in both chambers was kept at 1×10^{-9} mbar. Non-monochromatized Al K_α line at 1486.6 eV and an analyzer pass energy of 97 eV, giving a full width at half maximum (FWHM) of 1.7 eV for the Au $4f_{7/2}$ peak, were employed in all XPS studies. The XPS core level spectra were analyzed using a fitting routine, which can decompose each spectrum into individual mixed Gaussian-Lorentzian peaks after a Shirley background subtraction. The calibration of the analyzer's kinetic energy scale was accomplished according to ASTM-E 902–88. The binding energy (BE) scale was calibrated by attributing the main C1s peak at 284.8 (adventitious carbon) eV. The powdered samples were pressed into pellets with a thickness of 1 mm and 1 cm diameter before being introduced into the ultrahigh vacuum system.

4.3. Catalytic Activity Measurements

The apparatus used to perform the ESR experiments has been already described in our previous relevant studies regarding the iso-octane steam reforming over Cu supported on rare earth oxides

catalysts [48,93]. In brief, it is comprised of: (i) a liquid reactants feed unit equipped with He mass flow controllers and the gas-liquid saturator units; (ii) a fixed bed U-shaped quartz tubular reactor (9.6 mm, i.d.) loaded with 250 mg catalyst admixed with an equal amount of quartz particles and (iii) a gas analysis system.

A mixture of ethanol and water vapors of different steam-to-carbon (S/C) molar ratios was introduced into the reactor by bubbling He (99.999% purity, Air Liquid) through two separate vessels containing liquid C_2H_5OH (99.5% purity, Riedel-de Haen) and twice distilled water. The S/C feed ratio was adjusted by controlling the temperature and He-bubbled flow in the H_2O and ethanol saturators (based on their corresponding vapor pressures). The inlet volumetric flow rate was held constant at 150 cm^3/min, corresponding to a weight/flow (W/F) and Gas Hourly Space Velocity (GHSV) of 0.1 g.s/cm^3 and 21,000 h^{-1} (based on a catalyst bed volume of about 0.45 cm^3), respectively. The feed concentration used during the activity and stability experiments is: P_{EtOH} = 2 kPa, P_{H2O} = 2, 6, 12, 24 kPa, corresponding to a S/C feed ratio of 0.5, 1.5, 3, 6, respectively. Short-term durability experiments were performed by continuously monitoring the product rate as a function of time-on-stream (TOS, 24 h) at three different temperatures, *i.e.*, 400, 600, and 800 °C.

An on-line gas chromatograph (HP 6890), equipped with thermal conductivity and flame ionization detectors, was employed to qualitatively and quantitatively analyze reactants and products. The separation of H_2, CH_4, and CO was achieved with a Molecular Sieve 5A column (10 ft × 1/8 in), whereas CO_2, H_2O, C_2H_4, C_2H_6, C_2H_5OH, CH_3CHO and CH_3COCH_3 were separated in a Poraplot Q column (10 ft × 1/8 in) in a series bypass configuration.

The equations used to calculate the ethanol conversion (X_{EtOH}), product selectivity (S_i), and yield (Y_i), have as follows:

$$X_{EtOH}\,(\%) = \frac{[EtOH]_{inlet} - [EtOH]_{outlet}}{[EtOH]_{inlet}} \times 100 \quad (10)$$

$$S_i = \frac{r_i}{\sum r_i} \quad (11)$$

$$Y_i = X_{EtOH} * S_i \quad (12)$$

where [EtOH] denotes the ethanol concentration and r_i the formation rate of product i (mol/s) considering the following produced chemical species: H_2, CO, CO_2, CH_4, C_2H_4, C_2H_6, CH_3CHO, CH_3COCH_3.

The formation rate of product i, r_i, is calculated on the basis of its % v/v concentration in the reactor outlet, according to the equation:

$$r_i(mol/s) = \frac{\text{Concentration}\,(\%v/v)\cdot F_T\,(cm^3/min)}{100\cdot 60\,(s/min)\cdot v_m\,(cm^3/mol)} \quad (13)$$

where F_T, is the total flow rate and v_m, is the gas molar volume at STP conditions (298 K and 1 bar).

5. Conclusions

In the present work, the steam reforming of ethanol over transition metal catalysts (Fe, Co, Ni, Cu) supported on CeO_2 was examined. Various parameters, concerning the effect of operation temperature, steam-to-carbon ratio, and metal loading on the catalytic activity and stability were explored. The optimal catalytic performance was observed for the 20 wt.% Co/CeO_2 catalyst, which offers H_2 yields up to 66% at a steam-to-carbon feed ratio of 3. Stability experiments demonstrated the excellent stability of Co/CeO_2 catalysts in the temperature range of 400–800 °C. An inferior stability performance, particularly at low temperatures, was observed for all the other tested catalysts, following the order: Co >Ni >Cu >Fe. The excellent stability of Co/CeO_2 catalysts can be mainly assigned to the strong metal-support interactions which in turn leads to an increased population of surface oxygen species, related to lattice oxygen in ceria and cobalt oxides. This factor is thought to be

responsible for the facile gasification of the adsorbed species, thus preventing catalyst deactivation. The enhanced performance of Co-based catalysts, compared to a conventional Ni-based catalyst, is of major importance towards the direct utilization of ethanol in SOFCs, where highly active and robust electro-catalysts need to be developed.

Acknowledgments: This research was supported by the European Union (European Social Fund—ESF) and Greek national funds through the Operational Program "Education and Lifelong Learning" of the National Strategic Reference Framework (NSRF)—Research Funding Program: Heracleitus II. Investing in knowledge society through the European Social Fund. The Laboratory of Surface Characterization at FORTH/ICE-HT in Patras, Greece, is acknowledged for performing the XPS measurements.

Author Contributions: M.K. and G.M. conceived and designed the project. M.K. participated in the analysis and interpretation of characterization results. Tz.K. performed catalysts synthesis, whereas Z.I. carried out catalyst characterization and evaluation. The manuscript was written through the contribution of all authors. All authors approved the final version of the manuscript.

Conflicts of Interest: The authors declare no conflict of interest.

References

1. Goltsov, V.A.; Veziroglu, T.N.; Goltsova, L.F. Hydrogen civilization of the future—A new conception of the IAHE. *Int. J. Hydrogen Energy* **2006**, *31*, 153–159. [CrossRef]
2. Ni, M.; Leung, D.Y.C.; Leung, M.K.H.; Sumathy, K. An overview of hydrogen production from biomass. *Fuel Process. Technol.* **2006**, *87*, 461–472. [CrossRef]
3. Ni, M.; Leung, M.K.H.; Sumathy, K.; Leung, D.Y.C. Potential of renewable hydrogen production for energy supply in Hong Kong. *Int. J. Hydrogen Energy* **2006**, *31*, 1401–1412. [CrossRef]
4. Ni, M.; Leung, M.K.H.; Leung, D.Y.C.; Sumathy, K. A review and recent developments in photocatalytic water-splitting using TiO_2 for hydrogen production. *Renew. Sustain. Energy Rev.* **2007**, *11*, 401–425. [CrossRef]
5. Galbe, M.; Zacchi, G.A. A review of the production of ethanol from softwood. *Appl. Microbiol. Biotechnol.* **2002**, *59*, 618–628. [CrossRef] [PubMed]
6. Dien, B.S.; Cotta, M.A.; Jeffries, T.W. Bacteria engineered for fuel ethanol production: Current Status. *Appl. Microbiol. Biotechnol.* **2003**, *63*, 258–266. [CrossRef] [PubMed]
7. Sun, Y.; Cheng, J.Y. Hydrolysis of lignocellulosic materials for ethanol production: A Review. *Bioresour. Technol.* **2002**, *83*, 1–11. [CrossRef]
8. Cai, W.; Wang, F.; van Veen, A.C.; Provendier, H.; Mirodatos, C.; Shen, W. Autothermal reforming of ethanol for hydrogen production over an Rh/CeO_2 catalyst. *Catal. Today* **2008**, *138*, 152–156. [CrossRef]
9. Zhang, B.; Tang, X.; Li, Y.; Xu, Y.; Shen, W. Hydrogen production from steam reforming of ethanol and glycerol over ceria-supported metal catalysts. *Int. J. Hydrogen Energy* **2006**, *32*, 2367–2373. [CrossRef]
10. Ni, M.; Leung, D.Y.C.; Leung, M.K.H. A review on reforming bio-ethanol for hydrogen production. *Int. J. Hydrogen Energy* **2007**, *32*, 3238–3247. [CrossRef]
11. Nishiguchi, T.; Matsumoto, T.; Kanai, H.; Utani, K.; Matsumura, Y.; Shen, W.J.; Imamura, S. Catalytic steam reforming of ethanol to produce hydrogen and acetone. *Appl. Catal. A* **2005**, *279*, 273–277. [CrossRef]
12. Contreras, J.L.; Salmones, J.; Colin-Luna, J.A.; Nuno, L.; Quintana, B.; Cordova, I.; Zeifert, B.; Tapia, C.; Fuentes, G.A. Catalysts for H_2 production using the ethanol steam reforming (a review). *Int. J. Hydrogen Energy* **2014**, *39*, 18835–18853. [CrossRef]
13. Haryanto, H.; Fernando, S.; Murali, N.; Adhikari, S. Current Status of Hydrogen Production Techniques by Steam Reforming of Ethanol: A Review. *Energy Fuels* **2005**, *19*, 2098–2106. [CrossRef]
14. Frusteri, F.; Freni, S.; Spadaro, L.; Chiodo, V.; Bonura, G.; Donato, S.; Cavallaro, S. H_2 production for MC fuel cell by steam reforming of ethanol over MgO supported Pd, Rh, Ni and Co catalysts. *Catal. Commun.* **2004**, *5*, 611–615. [CrossRef]
15. Erdohelyi, A.; Rasko, J.; Kecskes, T.; Toth, M.; Domok, M.; Baan, K. Hydrogen formation in ethanol reforming on supported noble metal catalysts. *Catal. Today* **2006**, *116*, 367–376. [CrossRef]
16. Liguras, D.K.; Kondarides, D.I.; Verykios, X.E. Production of hydrogen for fuel cells by steam reforming of ethanol over supported noble metal catalysts. *Appl. Catal. B* **2003**, *43*, 345–354. [CrossRef]
17. Cavallaro, S.; Chiodo, V.; Freni, S.; Mondello, N.; Frusteri, F. Performance of Rh/Al_2O_3 catalyst in the steam reforming of ethanol: H_2 Production for MCFC. *Appl. Catal. A* **2003**, *249*, 119–128. [CrossRef]

18. Diagne, C.; Idriss, H.; Pearson, K.; Gomez-Garcia, M.A.; Kiennemann, A.R. Efficient hydrogen production by ethanol reforming over Rh catalysts effect of addition of Zr on CeO_2 for the oxidation of CO to CO_2. *C.R. Chim.* **2004**, *7*, 617–622. [CrossRef]
19. Mathure, P.V.; Ganguly, S.; Patwardhan, A.V.; Saha, R.K. Steam reforming of ethanol using a commercial nickel-based catalyst. *Ind. Eng. Chem. Res.* **2007**, *46*, 8471–8479. [CrossRef]
20. Konsolakis, M.; Ioakeimidis, Z. Surface/structure functionalization of copper-based catalysts by metal-support and/or metal–metal interactions. *Appl. Surf. Sci.* **2014**, *320*, 244–255. [CrossRef]
21. Gates, S.M.; Russell, J.N.; Yates, J.T. Bond activation sequence observed in the chemisorption and surface reaction of ethanol on Ni(lll). *Surf. Sci.* **1986**, *171*, 111–134. [CrossRef]
22. Sehested, J. Four challenges for nickel steam-reforming catalysts. *Catal. Today* **2006**, *111*, 103–110. [CrossRef]
23. Patel, M.; Jindal, T.K.; Pant, K.K. Kinetic Study of steam reforming of ethanol on Ni-Based ceria—Zirconia catalyst. *Ind. Eng. Chem. Res.* **2013**, *52*, 15763–15771. [CrossRef]
24. Homs, N.; Llorca, J.; Ramírez de la Piscina, P. Low-temperature steam-reforming of ethanol over ZnO-supported Ni and Cu catalysts: The Effect of Nickel and Copper Addition to ZnO-Supported Cobalt-Based Catalysts. *Catal. Today* **2006**, *116*, 361–336. [CrossRef]
25. Xu, W.; Liu, Z.; Johnston-Peck, A.C.; Senanayake, S.D.; Zhou, G.; Stacchiola, D.J.; Stach, E.A.; Rodriguez, J.A. Steam reforming of ethanol on Ni/CeO_2: Reaction Pathway and Interaction between Ni and the CeO_2 Support. *ACS Catal.* **2013**, *3*, 975–984. [CrossRef]
26. Senanayake, S.D.; Evans, J.; Agnoli, S.; Barrio, L.; Chen, T.-L.; Hrbek, J.; Rodriguez, J.A. Water–gas shift and CO methanation reactions over Ni–CeO_2(111) catalysts. *Top. Catal.* **2011**, *54*, 34–41. [CrossRef]
27. Carrasco, J.; Lopez-Duran, D.; Liu, Z.; Duchon, T.; Evans, J.; Senanayake, S.D.; Crumlin, E.J.; Matolin, V.; Rodriguez, J.A.; Ganduglia-Pirovano, M.V. *In situ* and theoretical studies for the dissociation of water on an active Ni/CeO_2 catalyst: Importance of Strong Metal–Support Interactions for the Cleavage of O–H Bonds. *Angew. Chem. Int. Ed.* **2015**, *54*, 1–6. [CrossRef] [PubMed]
28. Polychronopoulou, K.; Kalamaras, C.M.; Efstathiou, A.M. Ceria-Based Materials for Hydrogen Production Via Hydrocarbon Steam Reforming and Water-Gas Shift Reactions. *Rec. Pat. Mat. Sci.* **2011**, *4*, 122–145. [CrossRef]
29. Ilieva, L.; Pantaleo, G.; Sobczak, J.W.; Ivanov, I.; Venezia, A.M.; Andreev, D. NO reduction by CO in the presence of water over gold supported catalysts on CeO_2_Al_2O_3 mixed support, prepared by mechanochemical activation. *Appl. Catal. B* **2007**, *76*, 107–114. [CrossRef]
30. Baudin, F.; da Costa, P.; Thomas, C.; Calvo, S.; Lendresse, Y.; Schneider, S.; Delacroix, F.; Plassat, G.; Mariadassou, G.D. NO_x reduction over CeO_2-ZrO_2 supported iridium catalyst in the presence of propanol. *Top. Catal.* **2004**, *30/31*, 97–101. [CrossRef]
31. De Lima, S.M.; da Cruz, I.O.; Jacobs, G.; Davis, B.H.; Mattos, L.V.; Noronha, F.B. Steam reforming, partial oxidation, and oxidative steam reforming of ethanol over $Pt/CeZrO_2$ catalyst. *J. Catal.* **2008**, *257*, 356–368. [CrossRef]
32. Laosiripojana, N.; Assabumrungrat, S. Catalytic steam reforming of ethanol over high surface area CeO_2: The Role of CeO_2 as an Internal Pre-Reforming Catalyst. *Appl. Catal. B* **2006**, *66*, 29–39. [CrossRef]
33. Zhang, C.; Li, S.; Li, M.; Wang, S.; Ma, X.; Gong, J. Enhanced Oxygen Mobility and Reactivity for Ethanol Steam Reforming. *AIChE J.* **2012**, *58*, 516–525. [CrossRef]
34. Wang, H.; Liu, Y.; Wang, L.; Qin, Y. Study on the Carbon Deposition in Steam Reforming of Ethanol over Co/CeO_2 Catalyst. *Chem. Eng. J.* **2008**, *145*, 25–31. [CrossRef]
35. Song, H.; Ozkan, U.S. Changing the Oxygen Mobility in Co/Ceria Catalysts by Ca Incorporation: Implications for Ethanol Steam Reforming. *J. Phys. Chem. A* **2010**, *114*, 3796–3801. [CrossRef] [PubMed]
36. Song, H.; Ozkan, U.S. Ethanol steam reforming over Co-based catalysts: Role of Oxygen Mobility. *J. Catal.* **2009**, *261*, 66–74. [CrossRef]
37. Llorca, J.; Homs, N.; Sales, J.; Ramirez de la Piscina, P. Efficient production of hydrogen over supported cobalt catalysts from Ethanol Steam Reforming. *J. Catal.* **2002**, *209*, 306–317. [CrossRef]
38. Llorca, J.; Ramirez de la Piscina, P.; Dalmonb, J.-A.; Sales, J.; Homs, N. CO-free hydrogen from steam-reforming of bioethanol over ZnO-supported cobalt catalysts. Effect of the metallic precursor. *Appl. Catal. B* **2003**, *43*, 355–369. [CrossRef]

39. Casanovas, A.; Roig, M.; de Leitenburg, C.; Trovarelli, A.; Llorca, J. Ethanol steam reforming and water gas shift over Co/ZnO catalytic honeycombs doped with Fe, Ni, Cu, Cr and Na. *Int. J. Hydrogen Energy* **2010**, *35*, 7690–7698. [CrossRef]
40. Song, H.; Zhang, L.; Watson, R.B.; Braden, D.; Ozkan, U.S. Investigation of bio-ethanol steam reforming over cobalt-based catalysts. *Catal. Today* **2007**, *129*, 346–354. [CrossRef]
41. Soykal, I.I.; Sohn, H.; Ozkan, U.S. Effect of Support Particle Size in Steam Reforming of Ethanol over Co/CeO_2 Catalysts. *ACS Catal.* **2012**, *2*, 2335–2348. [CrossRef]
42. Espinal, R.; Taboada, E.; Molins, E.; Chimentao, R.J.; Medina, F.; Llorca, J. Cobalt hydrotalcites as catalysts for bioethanol steam reforming. The promoting effect of potassium on catalyst activity and long-term stability. *Appl. Catal. B* **2012**, *127*, 59–67. [CrossRef]
43. Espinal, R.; Anzola, A.; Adrover, E.; Roig, M.; Chimentao, R.; Medina, F.; Lopez, E.; Borio, D.; Llorca, J. Durable ethanol steam reforming in a catalytic membrane reactor at moderate temperature over cobalt hydrotalcite. *Int. J. Hydrogen Energy* **2014**, *39*, 10902–10910. [CrossRef]
44. Espinal, R.; Taboada, E.; Molins, E.; Chimentao, R.J.; Medina, F.; Llorca, J. Ethanol Steam reforming over hydrotalcite-derived Co Catalysts doped with Pt and Rh. *Top. Catal.* **2013**, *56*, 1660–1671. [CrossRef]
45. Ferencz, Z.; Erdőhelyi, A.; Baán, K.; Oszkó, A.; Óvári, L.; Kónya, Z.; Papp, C.; Steinrück, H.-P.; Kiss, J. Effects of support and Rh additive on Co-based catalysts in the ethanol steam reforming reaction. *ACS Catal.* **2014**, *4*, 1205–1218. [CrossRef]
46. Varga, E.; Ferencz, Z.; Oszkó, A.; Erdőhelyi, A.; Kiss, J. Oxidation states of active catalytic centers in ethanol steam reforming reaction on ceria based Rh promoted Co catalysts: An XPS Study. *J. Mol. Catal. A* **2015**, *397*, 127–133. [CrossRef]
47. Gamarra, D.; Munuera, G.; Hungría, A.B.; Fernández-García, M.; Conesa, J.C.; Midgley, P.A.; Wang, X.Q.; Hanson, J.C.; Rodríguez, J.A.; Martínez-Arias, A. Structure-activity relationship in nanostructured copper-ceria-based preferential CO oxidation catalysts. *J. Phys. Chem. C* **2007**, *111*, 11026–11038. [CrossRef]
48. Al-Musa, A.; Al-Saleh, M.; Ioakimidis, Z.; Ouzounidou, M.; Yentekakis, I.V.; Konsolakis, M.; Marnellos, G.E. Hydrogen production by iso-octane steam reforming over Cu catalysts supported on Rare Earth Oxides (REOs). *Int. J. Hydrogen Energy* **2014**, *39*, 1350–1363. [CrossRef]
49. Breen, B.; Ross, J.R.H. Methanol reforming for fuel-cell applications: Development of Zirconia-Containing Cu-Zn-Al Catalysts. *Catal. Today* **1999**, *511*, 521–533. [CrossRef]
50. Turco, M.; Bagnasco, G.; Cammarano, C.; Senese, P.; Costantino, U.; Sisani, M. $Cu/ZnO/Al_2O_3$ catalysts for oxidative steam reforming of methanol: The Role of Cu and the Dispersing Oxide Matrix. *Appl. Catal. B* **2007**, *77*, 46–57. [CrossRef]
51. Tang, X.; Zhang, B.; Li, Y.; Xu, Y.; Xin, Q.; Shen, W. CuO/CeO_2 catalysts: Redox Features and Catalytic Behaviors. *Appl. Catal. A* **2005**, *288*, 116–125. [CrossRef]
52. Papavasiliou, J.; Avgouropoulos, G.; Ioannides, T. Effect of dopants on the performance of $CuO\text{-}CeO_2$ catalysts in methanol steam reforming. *Appl. Catal. B* **2007**, *69*, 226–234. [CrossRef]
53. Konsolakis, M.; Sgourakis, M.; Carabineiro, S.A.C. Surface and redox properties of cobalt–ceria binary oxides: On the Effect of Co Content and Pretreatment Conditions. *Appl. Surf. Sci.* **2015**, *341*, 48–54. [CrossRef]
54. Zhang, C.; Li, S.; Wu, G.; Gong, J. Synthesis of stable $Ni\text{-}CeO_2$ catalysts via ball-milling for ethanol steam reforming. *Catal. Today* **2014**, *233*, 53–60. [CrossRef]
55. Shan, W.; Luo, M.; Ying, P.; Shen, W.; Can, L. Reduction property and catalytic activity of $Ce_{1-x}Ni_xO_2$ mixed oxide catalysts for CH_4 oxidation. *Appl. Catal. A* **2003**, *246*, 1–9. [CrossRef]
56. Zhang, B.; Tang, X.; Li, Y.; Cai, W.; Xu, Y.; Shen, W. Steam reforming of bio-ethanol for the production of hydrogen over ceria-supported Co, Ir and Ni catalysts. *Catal. Commun.* **2006**, *7*, 367–372. [CrossRef]
57. Frusteri, F.; Freni, S.; Chiodo, V.; Donato, S.; Bonura, G.; Cavallaro, S. Steam and auto-thermal reforming of bio-ethanol over MgO and CeO_2 Ni supported catalysts. *Int. J. Hydrogen Energy* **2006**, *31*, 2193–2199. [CrossRef]
58. Perez-Alonso, F.J.; Melián-Cabrera, I.; López Granados, M.; Kapteijn, F.; Fierro, J.L.G. Synergy of $Fe_xCe_{1-x}O_2$ mixed oxides for N_2O decomposition. *J. Catal.* **2006**, *239*, 340–346. [CrossRef]
59. Jin, Y.; Datye, A.K. Phase Transformations in Iron Fischer-Tropsch catalysts during temperature-programmed reduction. *J. Catal.* **2000**, *196*, 8–17. [CrossRef]
60. Voskoboinikov, T.V.; Chen, H.Y.; Sachtler, W.M.H. On the nature of active sites in Fe/ZSM-5 catalysts for NO_x abatement. *Appl. Catal. B* **1998**, *19*, 279–287. [CrossRef]

61. Gálvez, M.E.; Ascaso, S.; Stelmachowsk, P.; Legutko, P.; Kotarba, A.; Moliner, R.; Lázaro, M.J. Influence of the surface potassium species in Fe-K/Al_2O_3 catalysts on the soot oxidation activity in the presence of NO_x. *Appl. Catal. B* **2014**, *152–153*, 88–98. [CrossRef]
62. Reddy, G.K.; Boolchand, P.; Smirniotis, P.G. Sulfur tolerant metal doped Fe/Ce catalysts for high temperature WGS reaction at low steam to CO ratios—XPS and Mössbauer spectroscopic study. *J. Catal.* **2011**, *282*, 258–269. [CrossRef]
63. Zyryanova, M.M.; Snytnikov, P.V.; Gulyaev, R.V.; Amosov Yu, I.; Boronin, A.I.; Sobyanin, V.A. Performance of Ni/CeO_2 catalysts for selective CO methanation in hydrogen-rich gas. *Chem. Eng. J.* **2014**, *238*, 189–197. [CrossRef]
64. Nesbitt, H.W.; Legrand, D.; Bancroft, G.M. Interpretation of Ni2p XPS spectra of Ni conductors and Ni insulators. *Phys. Chem. Miner.* **2000**, *27*, 357–366. [CrossRef]
65. Biesinger, M.C.; Payne, B.P.; Lau, L.W.M.; Gerson, A.; Smart, R.S.C. X-ray photoelectron spectroscopic chemical state quantification of mixed nickel metal, oxide and hydroxide systems. *Surf. Interface Anal.* **2009**, *41*, 324–332. [CrossRef]
66. Kundakovic, L.; Flytzani-Stephanopoulos, M. Reduction characteristics of copper oxide in cerium and zirconium oxide systems. *Appl. Catal. A* **1998**, *171*, 13–29.
67. Li, W.; Flytzani-Stephanopoulos, M. Total Oxidation of Carbon-Monoxide and Methane over Transition Metal Fluorite Oxide Composite Catalysts: II. Catalyst Characterization and Reaction-Kinetics. *J. Catal.* **1995**, *153*, 317–332. [CrossRef]
68. Ayastuy, J.L.; Gurbani, A.; González-Marcos, M.P.; Gutiérrez-Ortiz, M.A. Selective CO oxidation in H_2 streams on CuO/$Ce_xZr_{1-x}O_2$ catalysts: Correlation between Activity and Low Temperature Reducibility. *Int. J. Hydrogen Energy* **2012**, *37*, 1993–2006. [CrossRef]
69. Lamonier, C.; Bennani, A.; D'Huysser, A.; Aboukaïs, A.; Wrobel, G. Evidence for different copper species in precursors of copper-cerium oxide catalysts for hydrogenation reactions: An X-Ray Diffraction, EPR and X-Ray Photoelectron Spectroscopy Study. *Faraday Trans.* **1996**, *92*, 131–136. [CrossRef]
70. Mai, H.; Zhang, D.; Shi, L.; Li, H. Highly active $Ce_{1-x}Cu_xO_2$ nanocomposite catalysts for the low temperature oxidation of CO. *Appl. Surf. Sci.* **2011**, *257*, 7551–7559. [CrossRef]
71. Rao, K.N.; Venkataswamy, P.; Reddy, B.M. Structural Characterization and Catalytic Evaluation of Supported Copper–Ceria Catalysts for Soot Oxidation. *Ind. Eng. Chem. Res.* **2011**, *50*, 11960–11969. [CrossRef]
72. Santos, V.P.; Carabineiro, S.A.C.; Bakker, J.J.W.; Soares, O.S.G.P.; Chen, X.; Pereira, M.F.R.; Órfão, J.J.M.; Figueiredo, J.L.; Gascon, J.; Kapteijn, F. Stabilized gold on cerium-modified cryptomelane: Highly Active in Low-Temperature CO Oxidation. *J. Catal.* **2014**, *309*, 58–65. [CrossRef]
73. Varga, E.; Pusztai, P.; Óvári, L.; Oszkó, A.; Erdőhelyi, A.; Papp, C.; Steinrück, H.-P.; Kónya, Z.; Kiss, J. Probing the interaction of Rh, Co and bimetallic Rh–Co nanoparticles with the CeO_2 support: Catalytic Materials for Alternative Energy Generation. *Phys. Chem. Chem. Phys.* **2015**, *17*, 27154–27166. [CrossRef] [PubMed]
74. Vári, G.; Óvári, L.; Papp, C.; Steinrück, H.-P.; Kiss, J.; Kónya, Z. The Interaction of Cobalt with CeO_2(111) Prepared on Cu(111). *J. Phys. Chem. C* **2015**, *119*, 9324–9333. [CrossRef]
75. Ocampo, F.; Louis, B.; Roger, A.C. Methanation of carbon dioxide over nickel-based $Ce_{0.72}Zr_{0.28}O_2$ mixed oxide catalysts prepared by sol–gel method. *Appl. Catal. A* **2009**, *369*, 90–96. [CrossRef]
76. Palma, V.; Castaldo, F.; Ciambelli, P.; Iaquaniello, G. CeO_2-supported Pt/Ni catalyst for the renewable and clean H_2 production via ethanol steam reforming. *Appl. Catal. B Environ.* **2013**, *145*, 73–84. [CrossRef]
77. Carrero, A.; Calles, J.A.; Vizcaino, A.J. Hydrogen production by ethanol steam reforming over Cu-Ni/SBA-15 supported catalysts prepared by direct synthesis and impregnation. *Appl. Catal. A* **2007**, *327*, 82–94. [CrossRef]
78. Pang, X.; Chen, Y.; Dai, R.; Cui, P. Co/CeO_2 Catalysts Prepared Using Citric Acid Complexing for Ethanol Steam Reforming. *Chin. J. Catal.* **2012**, *33*, 281–289. [CrossRef]
79. Fatsikostas, A.N.; Verykios, X.E. Reaction network of steam reforming of ethanol over Ni-based catalysts. *J. Catal.* **2004**, *225*, 439–452. [CrossRef]
80. Fierro, V.; Akdim, O.; Mirodatos, C. On-board hydrogen production in a hybrid electric vehicle by bio-ethanol oxidative steam reforming over Ni and noble metal based catalysts. *Green Chem.* **2003**, *5*, 20–24. [CrossRef]
81. Mariño, F.; Boveri, M.; Baronetti, G.; Laborde, M. Hydrogen production from steam reforming of bioethanol using Cu/Ni/K/γ-Al_2O_3 catalysts. Effect of Ni. *Int. J. Hydrogen Energy* **2001**, *26*, 665–668. [CrossRef]

82. Melnick, J.G.; Radosevich, A.T.; Villagrán, D.; Nocera, D.G. Decarbonylation of ethanol to methane, carbon monoxide and hydrogen by a [PNP]Ir complex. *Chem. Commun.* **2010**, *46*, 79–81. [CrossRef] [PubMed]
83. Agus, H.; Sandun, F.; Naveen, M.; Sushil, A. Current Status of Hydrogen Production Techniques by Steam Reforming of Ethanol: A Review. *Energy Fuels* **2005**, *19*, 2098–2106.
84. Sadykov, V.; Mezentseva, N.; Alikina, G.; Bunina, R.; Pelipenko, V.; Lukashevich, A.; Vostrikov, Z.; Rogov, V.; Krieger, T.; Ishchenko, A.; *et al*. Nanocomposite Catalysts for Steam Reforming of Methane and Biofuels: Design and Performance. In *Advances in Nanocomposites—Synthesis, Characterization and Industrial Applications*; Reddy, B.S.R., Ed.; In Tech: Rijeka, Croatia, 2011; pp. 909–946.
85. De Lima, S.M.; da Silva, A.M.; da Costa, L.O.O.; Graham, U.M.; Jacobs, G.; Davis, B.H.; Mattos, L.V.; Noronha, F.B. Study of catalyst deactivation and reaction mechanism of steam reforming, partial oxidation, and oxidative steam reforming of ethanol over Co/CeO_2 catalyst. *J. Catal.* **2009**, *268*, 268–281. [CrossRef]
86. Galetti, A.E.; Gomez, M.F.; Arrua, L.A.; Marchi, A.J.; Abello, M.C. Study of CuCoZnAl oxide as catalyst for the hydrogen production from ethanol reforming. *Catal. Commun.* **2008**, *9*, 1201–1208. [CrossRef]
87. Wang, H.; Liu, Y.; Wang, L.; Qin, Y.N. Study on the carbon deposition in steam reforming of ethanol over Co/CeO_2 catalyst. *Chem. Eng. J.* **2008**, *145*, 25–31. [CrossRef]
88. Yu, S.W.; Huang, H.H.; Tang, C.W.; Wang, C.B. The effect of accessible oxygen over Co_3O_4-CeO_2 catalysts on the steam reforming of ethanol. *Int. J. Hydrogen Energy* **2014**, *39*, 20700–20711. [CrossRef]
89. Moon, D.J. Hydrogen production by catalytic reforming of liquid hydrocarbons. *Catal. Surv. Asia* **2011**, *15*, 25–36. [CrossRef]
90. Finocchio, E.; Rossetti, I.; Ramis, G. Redox properties of Co- and Cu-based catalysts for the steam reforming of ethanol. *Int. J. Hydrogen Energy* **2013**, *38*, 3213–3225. [CrossRef]
91. Da Silva, A.M.; de Souza, K.R.; Mattos, L.V.; Jacobs, G.; Davis, B.H.; Noronha, F.B. The effect of support reducibility on the stability of Co/CeO_2 for the oxidative steam reforming of ethanol. *Catal. Today* **2011**, *164*, 234–239. [CrossRef]
92. Mosqueda, B.; Toyir, J.; Kaddouri, A.; Gelin, P. Steam reforming of methane under water deficient conditions over gadolinium doped ceria. *Appl. Catal. B* **2009**, *88*, 361–367. [CrossRef]
93. Al-Musa, A.A.; Ioakeimidis, Z.S.; Al-Saleh, M.S.; Al-Zahrany, A.; Marnellos, G.E.; Konsolakis, M. Steam reforming of iso-octane toward hydrogen production over mono- and bi-metallic Cu-Co/CeO_2 catalysts: Structure-Activity Correlations. *Int. J. Hydrogen Energy* **2014**, *39*, 19541–19554. [CrossRef]
94. Cai, W.; Wang, F.; Daniel, C.; van Veen, A.C.; Schuurman, Y.; Descorme, C.; Provendier, H.; Shen, W.; Mirodatos, C. Oxidative steam reforming of ethanol over Ir/CeO_2 catalysts: A Structure Sensitivity Analysis. *J. Catal.* **2012**, *286*, 137–152. [CrossRef]
95. Singhto, W.; Laosiripojana, N.; Assabumrungrat, S.; Charojrochkul, S. Steam reforming of bio-ethanol over Ni on Ce-ZrO_2 support: Influence of Redox Properties on the Catalyst Reactivity. *J. Sci. Technol.* **2006**, *28*, 1251–1264.
96. Laosiripojana, N.; Kiatkittipong, W.; Charojrochkul, S.; Assabumrungrat, S. Effects of support and co-fed elements on steam reforming of palm fatty acid distillate (PFAD) over Rh-based catalysts. *Appl. Catal. A* **2010**, *383*, 50–57. [CrossRef]
97. Salazar-Villalpando, M.D.; Berry, D.A.; Cugini, A. Role of lattice oxygen in the partial oxidation of methane over Rh/zirconia-doped ceria. Isotopic studies. *Int. J. Hydrogen Energy* **2010**, *35*, 1998–2003. [CrossRef]
98. Huang, T.J.; Wang, C.H. Roles of Surface and Bulk Lattice Oxygen in Forming CO_2 and CO during Methane Reaction over Gadolinia-Doped Ceria. *Catal. Lett.* **2007**, *118*, 103–108. [CrossRef]